MATERIALS CHEMISTRY
FRONTIERS

Accepted Manuscript

This article can be cited before page numbers have been issued, to do this please use: H. Zhang, R. Li, M. Humayun, Z. Huang, Y. Fu, Y. Yu, J. Duan, Y. A. Attia and C. Wang, *Mater. Chem. Front.*, 2024, DOI: 10.1039/D4QM00312H.

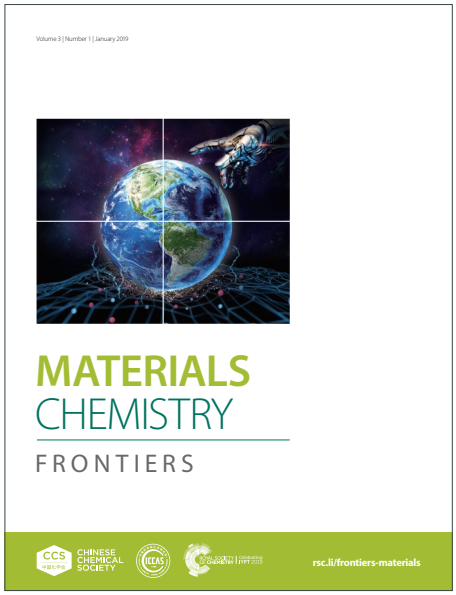

View Article Online
DOI: 10.1039/D4QM00312H

Recent progress in Mott-Schottky junction electrocatalysts for pH universal hydrogen evolution reaction

Huaming Zhang*[a], Rong Li[a], Muhammad Humayun[b], Zhihan Huang[a], Yanjun Fu[a], Yulin Cao[c], Junhong Duan[a], Yasser A. Attia[d], Chundong Wang*[e, b]

[a] Key Laboratory of Optoelectronic Information Perception and Instrumentation of Jiangxi Province, Nanchang Hangkong University, Nanchang 330063, Jiangxi, P.R. China

[b] Energy, Water, and Environment Lab, College of Humanities and Sciences, Prince Sultan University, Riyadh 11586, Saudi Arabia

[c] Physics Laboratory, School of Undergraduate Education, Shenzhen Polytechnic University, Shenzhen, 518055, P.R. China

[d] National Institute of Laser Enhanced Sciences, Cairo University, Giza 12613, Egypt

[e] School of Integrated Circuits, Wuhan National Laboratory for Optoelectronics, Huazhong University of Science and Technology, Wuhan 430074, P.R. China

Email: Huaming Zhang (70451@nchu.edu.cn); Chundong Wang (apcdwang@hust.edu.cn)

DOI: 10.1039/D4QM00312H

Abstract

The development of efficient electrocatalysts to reduce the overpotential for pH-universal hydrogen evolution reaction (HER) is necessary for the large-scale industrialization of hydrogen energy. Over the past several decades, a large number of preparation strategies for efficient electrocatalysts have been developed, and various exploration has been made to improve the mass transport and expose more active sites. Electrostatic potential energy at the Mott-Schottky heterojunction interface formed by electron transfer between metal and semiconductor can effectively regulate the electronic structure of the catalyst, provides more new active sites and accelerates charge transfer, in which the built-in electric field promotes local charge polarization at the heterojunction interface, and greatly improves the adsorption of the critical reaction intermediates, leading to enhanced electrocatalytic activity. This paper reviews the recent research progress of Mott-Schottky heterogeneous electrocatalysts, more detail of which can be summarized as follows: a) the formation mechanism of Mott-Schottky heterogeneous catalysts; b) Mott-Schottky effects on the interfacial charge distribution, d-band center and hydrogen adsorption energy are introduced; c) the effects of Mott-Schottky heterostructures on the catalytic performance are systematically discussed; d) challenges and prospects are given. This review can provide a deep understanding of the microscopic mechanism of Mott-Schottky heterogeneous catalysis and can be extended to design other transition metal-based catalysts.

Contents

1. Introduction

Fossil fuels have traditionally been the dominant energy source for driving industrial and commercial growth. Considering escalating energy consumption and associated environmental concerns, we need to develop sustainable and eco-friendly alternatives to current fossil fuels [1]. The conversion and storage of renewable energy into chemically stable fuels is an important step toward mitigating future energy crises [2, 3]. Hydrogen (H_2) is an efficient energy alternative due to its high-quality energy carrier (142 MJ kg^{-1}) and low carbon footprint [4-6]. Currently, about 96% of H_2 production from fossil fuels, includes steam reforming, partial oxidation, pyrolysis, and coal gasification. However, these techniques are severely hampered by its high cost and the emission of air pollutants [7, 8]. Developing sustainable and pollution-free techniques to produce high-quality H_2 is critical. Given the abundance of readily available water resources and low environmental pollution, electrochemical water splitting widely been regarded as a simple technology capable of converting and storing intermittent electricity produced by wind turbine or solar panel into valuable fuel, specifically hydrogen (H_2), in a sustainable manner [9, 10]. As revealed in Figure 1, The water electrolysis system includes an electrolytic tank, which formed by a cathode and an anode. The cathode is the component of electrochemical cell where the hydrogen evolution process (HER) occurs, while anode is component of electrochemical cell where the oxygen evolution reaction (OER) occurs concurrently [11]. Despite being studied for over 230 years, the use of water electrolysis for hydrogen prodction is now limited to small-scale operations due to the electrolytic cell's high cost and energy requirements. Furthermore, it only accounts for about 4% of overall hydrogen production [12]. The theory decomposition voltage for electrolytic water is 1.23 volt. In practice, extra input voltages (η) are required to overcome the energy barrier of the anode and cathode, resulting in water splitting. Typically, the process runs at a realistic voltage range of 1.8-2.5 V, higher than the ideal value of 1.23

View Article Online
DOI: 10.1039/D4QM00312H

V [13-15]. As a result, high-efficiency electrocatalysts must be developed in order to reduce the overpotential and accelerate kinetics for energy-efficient hydrogen production[16].

Noble metals such as platinum (Pt), iridium (Ir), and ruthenium (Ru) are currently used as standard catalysts for the HER due to their favorable Gibbs free energy (ΔG) for hydrogen adsorption (e.g., ΔG_{H^*} = –0.09 eV for Pt). However, their popularity is restricted due to scarcity, expensive cost, and insufficient consistency [17, 18]. Furthermore, catalysts based on Pt show low HER efficiency in non-acidic conditions such as neutral and alkaline electrolytes. These efficiencies are often 2-3 orders of magnitude lower than those seen in acidic environments. This is mostly owing to the sluggish rate of water dissociation in neutral and alkaline solutions [19-21]. Efforts have been made to successfully develop electrocatalysts that are durable for HER over a broad pH renge. A variety of transition metal-based electrocatalysts, including transition metal hydroxides[22], sulfides[23], phosphides [24], oxides [25], nitrides [26, 27] and selenides [28] have recently been developed aiming to replace expensive noble electrocatalysts. Unfortunately, while most of these catalysts are good in breaking H-OH bonds, they are not suitable for converting adsorbed H_{ad} species into H_2 [29]. Furthermore, the pH of the environment affects the activity and stability of most of the transition metal electrocatalysts. This is due to changes in the kinetics of the HER and the catalysts' potential dissolution in strongly acidic or alkaline conditions [30-33], which poses significant challenges in practical application across a wide range of operating conditions. Determining the efficiency of catalysts across different pH ranges is thus an important aspect of catalyst design. This is necessary to reduce the decline in energy efficiency caused by the unavoidable pH changes that occur throughout the membrane-separated chamber and/or near the electrode. Furthermore, it is critical to meet the exclusive needs of numerous applications, which include microbial electrolysis, chloro-alkali electrolyzers, and overall water splitting. Furthermore, the goal of this research is to reduce costs and simplify the processing

complexities of water splitting systems.

View Article Online
DOI: 10.1039/D4QM00312H

Developing effective methods for modifying compositions and structures of catalytic materials is a promising strategy to address their limitations in terms of activity and stability over a large pH range. Heterostructures consisting of interfaces of two dissimilar materials can equilibrate the Fermi levels to the same value to boost charge transfer and extend the region of charge depletion, which will regulate the electronic structures or the band structures of the components[34, 35]. Therefore, heterostructured catalysts exhibit higher HER activities than the single counterpart, offers a promising strategy to enhance the HER activity in all mediums with different pH values. In addition, the synergistic effect between different components also remarkable contributes to boost HER kinetics of the heterostructure electrocatalysts. Particularly, a Mott-Schottky junction is a well-known phenomenon that happens at metal-semiconductor interface. The Mott-Schottky effect at the junction accelerates charge transfer across the interface, redistributes charges at the interface, and modulates the adsorption ability of reaction intermediates. As a result, the inherent activity of catalysts increases (Scheme 1). Recently, there has been an ongoing focus on studying Mott-Schottky junctions as a new technology to improve the catalytic performance of catalysts used in energy storage, artificial photosynthesis, water splitting, and other applications [36-40]. For example, Su and colleagues developed a Mott-Schottky catalyst Co@NC via capsulating Co nanoparticles in nitrogen-rich carbon shells [41]. The Co/NC contact induces the Mott-Schottky effect, which drastically affects the electron density of Cu nanoparticles. This modification improves the catalytic performance of Cu nanoparticles, allowing them to efficiently oxidize alcohols without the use of a base.

To date, numerous review articles have been published on Mott-Schottky catalysts for various applications [42, 43]. However, no effort has been made to write a review paper that may highlight progressive developments about design and fabrication of diverse Mott-Schottky electrocatalysts that

View Article Online
DOI: 10.1039/D4QM00312H

have suitable HER activities across the entire pH range. This review explores into detail about the basic structure of Mott-Schottky heterojunctions, as well as the basics and reaction mechanism of Mott-Schottky electrocatalysts for HER over a wide pH range. We start by providing a brief introduction to the reaction mechanisms as well as the application for HER in various pH media. Furthermore, it discusses current advances in the construction and implementation of cutting-edge Mott-Schottky electrocatalysts for the HER process at all pH levels. Finally, the challenge and prospects for Mott-Schottky electrocatalysts are discussed in terms of high-performance water splitting. This review provides an overview for optimizing HER of Mott-Schottky catalysts, which may lead to future advancements in the fabrication of electrocatalysts.

2. Fundamentals of Electrocatalytic Water Splitting

It's critical to explore the mechanism underlying the hydrogen evolution process in order to more clearly understand the rate of water splitting reaction. The entire water electrolysis process is represented by reaction step i.e., $2H_2O \rightarrow 2H_2 + O_2$, which is split into two half-reactions: OER and HER, occurs at the anode and the cathode, respectively [44-46]. With a Gibbs free energy of +273 kJ mol^{-1}, the ideal thermodynamic potential of overall water splitting under the RHE is 1.23 V [47, 48]. Nevertheless, the real voltage of electrolytic water is higher than the theoretical value due to limitations caused by dynamics' effect and undesirable system resistance (i.e., overpotential) [49]. Considering the different electrolytes in which water splittingtakes place, the water splitting reactions can be expressed as follows[50, 51]:

Total reaction:

$$2H_2O \rightarrow 2H_2 + O_2, \quad (1)$$

In an acidic electrolyte:

View Article Online
DOI: 10.1039/D4QM00312H

Cathode:$4H^+ + 4e^- \rightarrow 2H_2$,

Anode:$2H_2O \rightarrow 4H^+ + O_2 + 4e^-$ (2)

In an alkaline electrolyte:

Cathode: $2H_2O + 4e^- \rightarrow 2H_2 + 4OH^-$ (3)

Anode: $4OH \rightarrow 2H_2O + O_2 + 4e^-$ (4)

Fundamental concepts must be investigated for purpose of optimizing the reaction system and address the aforementioned concerns. Because of the relatively low kinetics, the mechanism of HER is highly dependent on pH conditions and is primarily affected by a shift from acidic to alkaline. So, let us begin by quickly introducing the HER mechanism at different pH values.

2.1. HER mechanism in different pH media

It is widely accepted that, in acidic environments, the HER at the surfaces of many catalysts occurs in two steps [19, 45, 52]. At the commencement of HER, an adsorbed hydrogen atom (H*) was formed when H^+ adsorption on the catalyst surface (here * represents an active site on the catalyst surface). Equation (1) refers to this technique as the Volmer or discharge stage. As stated in Eq. (2), a H* combines with an H^+ and an electron (e^-) to form an H_2 molecule. This approach is known as the Heyrovsky step or electrochemical desorption step. Alternatively, H_2 could be formed by combining two H* on the surface of catalyst, an approach known as the Tafel step or chemical desorption step (Eq. (3)).

$H^+ + e^- \rightarrow H^*$ (Volmer step) (5)

$H^* + H^+ + e^- \rightarrow H_2$ (Heyrovsky step) (6)

$H^* + H^* \rightarrow H_2$ (Tafel step) (7)

View Article Online
DOI: 10.1039/D4QM00312H

Based on the Sabatier principle,[53, 54] the adsorption strength between the catalyst and H* strongly determined the HER kinetics.[19]

In alkaline (or neutral) solutions, HER begins with the disintegration of H_2O molecules to provide protons due to the absence of H^+. This reaction occurs in both the Heyrovsky step (Eq. (6)) and the Volmer step (Eq. (5)) in alkaline HER, but the Tafel step is the same as in acid solutions.

$$H_2O + e^- \rightarrow H^* + OH^- \quad \text{(Volmer step)} \quad (8)$$

$$H_2O + e^- + H^* \rightarrow H_2 + OH^- \quad \text{(Heyrovsky step)} \quad (9)$$

$$H^* + H^* \rightarrow H_2 \quad \text{(Tafel step)} \quad (10)$$

In alkaline electrolytes, most catalysts have slower HER kinetics because producing protons requires more energy in an alkaline media. Alkaline HER activity is governed by an intricate equilibrium between the energy required to dissociate H_2O and the bonding energy of hydrogen intermediates (ΔG_{H^*}) [55]. Thus, an excellent way to design catalysts for alkaline HER is to promote water dissociation while keeping an adequate hydrogen adsorption energy. Figure 2 depicts the HER pathways in acidic and alkaline (or neutral) media, respectively [45].

2.2 Overpotential

The overpotential is the difference between the experimental potential and the predicted thermodynamic equilibrium potential (E_{RHE} = 1.23 V) of an electrochemical reaction, which is one of key parameters for evaluating the efficiency of water splitting [56]. Overpotential is caused by concentration and electrochemical polarization at the electrode [57]. The applied potential (E) for driving HER at a certain current (i) can be expressed by equation (7):

$$E = E_{RHE} + iR - \eta \quad (11)$$

Here, iR indicates the ohmic potential reduction caused by the electrochemical system's series

View Article Online
DOI: 10.1039/D4QM00312H

resistance (R). The reaction overpotential (η) measures electrochemical reactivity. It is evident that more electrical energy is necessary to overcome the intrinsic activation barriers during electrocatalysis. The primary purpose of constructing a catalyst is to reduce the overpotential. A lower value of η implies that the catalyst electrode is more active, resulting in a high power transfer efficiency for the electrochemical water splitting system [58]. In order to reduce non-Faradic current, the most commonly used sweep rates are 2 mV s^{-1}, 2 mV s^{-1} and 5 mV s^{-1}. Generally, overpotential can be acquired form the linear sweep voltammetry (LSV) with *i*R-correction. Electrocatalysts are typically assessed with an overpotential to achieve a 10 mA cm^{-2} current density [59].

2.3 Tafel Slope and Exchange Current Density

The slope of the linear component of a Tafel plot, or Tafel slope, is an important feature for understanding the mechanism and electrocatalytic kinetics of electrocatalytic processes. Tafel slope can be determined directly using the electrochemical workstation or indirectly via polarization curves. The Tafel slope can be calculated by re-plotting polarization data as overpotential *vs* current density [60]. The indicated overpotential corresponds with Tafel slopes and current density (*j*), which can be expressed by equation (8):

$$\eta = a + b\log(j) \quad (12)$$

The overpotential is represented by η, the Tafel slope by b, and the current density by j. The exchange current density (j_0) of a reaction is the current density at the equilibrium potential where the cathodic and anodic currents level off [61]. It is readable from the intersection of the X-axis and the extrapolated linear component of Tafel graphs. The value of j_0 represents the ability to transport electrons under equilibrium conditions, and it is highly correlated with catalyst intrinsic activity. The exchange current density primarily indicates the intrinsic activity of charge transfer between the

View Article Online
DOI: 10.1039/D4QM00312H

electrode and the electrolyte, and promoting the exchange current density is what it means to catalyze the process [62]. Catalysts with high catalytic activity commonly have a surface with a higher j_0. As a result, the j_0 reflects the inherent activity of catalysts, whereas the Tafel slope provides an in-depth knowledge of reaction principles. Of course, a low Tafel slope and a high j_0 are required for the ideal electrocatalyst.

2.4 Faradaic efficiency

It is possible to determine the overall water decomposition using Faradaic efficiency. It is the ratio of the overall charge in an external circuit to the charge consumed by reactants [13]. To estimate FE, the molar amount of hydrogen produced by empirically gas chromatography is compared to the predicted amount produced by galvanostatic electrolysis.

2.4 Turnover Frequency

The turnover frequency (TOF) is the number of the product molecule generated per active site inunit time, demonstrating the genuine activity of electrocatalysts. It can be expressed via the following equation:

$$\mathrm{TOF} = jA/zFn, \quad (13)$$

where "*j*" is current density, "*A*" denotes the working area of electrode, "*z*" represents the number of electron transfer per molecule generated, "*F*" is Faraday constant, and "*n*" represents the amount of material (mol). It is worth noted that not all active atoms are involved in catalytic reaction and the value of *n* is overestimated, leading to the inaccuracy of TOF value. Nevertheless, it can still provide valuable reference in catalytic activity comparison between different electrocatasts.

View Article Online
DOI: 10.1039/D4QM00312H

2.5 Electrocatalysts stability

It is believed to be a more fundamental electrocatalyst parameter for HER. It is typically measured via a chronopotentiometry experiment via potential variation, or through measuring current change vs. reaction time at a fixed potential. Multicurrent step chronopotentiometry can determine anything from 10 mA cm^{-2} to 100 mA cm^{-2} or even 1000 cm^{-2}, allowing for an in-depth assessment of durability. Another effective way for assessing stability is compared the LSV graphs before and after the electrochemical reaction, which allows for the easy identification of any apparent loss in stability. After 500-10,000 cycles of CV, this stability can be acquired by compared the polarization curves before and after each cycle.

3. Mott-Schottky junction induced by Metal/semiconductor contact

3.1 Construction of the Mott-Schottky junction

In solid-state physics, an electric junction occurs when a metal-semiconductor comes into contact. The semiconductor's bands bend to match the metal's work function (Φ), which is the minimum energy required to extract an electron from the electronic ground state in a material [63, 64]. In metal/n-type semiconductors, stacking or stitching of this two materials allow electron transfer across the interface, leading to the development of a Mott-Schottky junction (Figure 3) [65]. Figure 3 shows that band bending and Schottky-barrier (Φ_{SB}) formation when the n-type semiconductor work function (Φ_s) smaller than the metal work function (Φ_m). This is caused by electrons transferring from the semiconductor to the metal until the Fermi levels of the metal ($E_{F,\ m}$) and semiconductor ($E_{F,\ s}$) are matched. The Φ_{SB} allows for irreversible charge transport across the heterointerface, resulting in electron accumulation or depletion at the metal-semiconductor interface [66]. Obviously, the metal/semiconductor contact may result in a built-in electric field, with the semiconductor side

View Article Online
DOI: 10.1039/D4QM00312H

positively charged due to electrostatic induction and the metal side having a higher electron density. The depletion layer surrounds the semiconductor surface and contains fewer electrons than the semiconductor itself. When $\Phi_s > \Phi_m$ (right of Figure 3), electrons migrated from metal to semiconductor, accumulating near the semiconductor surface to form an accumulation layer.

In general, when $E_{F,\ m}$ is less than $E_{F,\ s}$, the free charge is transferred to the contacting metal side, and conversely. So, at metal-semiconductor interfaces, surface charge density can be modified by the Mott-Schottky junction, a phenomenon known as the Mott-Schottky effect in solid state physics. Obviously, the Mott-Schottky junction will optimize electron transit and reaction intermediate adsorption.

3.2 Mott-Schottky Mechanism

As previously stated, electrocatalytic reactions occur on the electrocatalysts' surfaces and/or interfaces. As a result, the atomic configurations and surface electronic structure of electrocatalysts govern their catalytic potential [67]. Numerous successful strategies have been achieved to adjust catalysts' electronic properties in order to boost their catalytic efficiency, including heteroatom doping, changes crystal facets (or shape), nanoscale engineering, and hybrid approaches [68]. Until now, one of the most effective strategies for development of highly active catalysts is to manage the catalyst's surface charge distribution by precise structural engineering.

Given that the inherent electric field at the Mott-Schottky junction facilitates electrons transfer across electrochemical interfaces and subsequent leads to the surface electrons redistribution, this presents a viable method for accelerating the electron transfer from the catalyst's surface to the reaction intermediate. The electron transfer can optimize the electrostatic properties at the fabricated interfaces as well as the catalytic performance of the heterostructure by generating extra active sites

View Article Online
DOI: 10.1039/D4QM00312H

with rapid charge transfer features. In the meantime, it lowers the reaction barrier of active centers to water dissociation and increases hydrogen binding energy. Furthermore, the Mott-Schottky interface significantly increases structural stability by preventing aggregation of the active nanoparticles during long-term electrochemical reactions—a vital component of maintaining high electrocatalytic efficiency. As a result, the development of Mott-Schottky heterojunction catalysts provides a strategy for increasing the overall efficacy and efficiency of electrochemical water splitting, especially in applications such as pH universal water splitting for generating hydrogen. For example, Fan and co-workers [69] synthesized a series of Pt-based Mott−Schottky junction electrocatalysts with different $\Delta\Phi$ (= $|\Phi_s - \Phi_m|$) by precisely controlling the oxidation state of cobalt oxide. Their found that the intensity value of built-in electric field increased with the enlarge difference of work function. The bigger built-in electric field was facilitate to accelerating the charge transfer and optimizing the hydrogen/hydroxide adsorption processes during HER. Hence, the inherent electric field from metal-semiconductor heterointerfaces proposes a guidance for the development of high performance HER electrocatalysts.

3.2.1 Synergistic effects of different components in heterostructure materials

One characteristic of heterostructure that distinguishes it from single-component materials is the synergistic effect caused by the existence of heterointerfaces and multicomponent materials [70]. The synergistic effect of heterostructures can maximize the advantages of each individual component while also providing a practical and effective technique for developing high-performance electrochemical devices [71, 72]. In addition, the energy band and electronic structure of the materials may change as a result of interfaces formed between different components [65]. In these heterostructures, interfacial bonding may act as an electron transport bridge. In addition to

View Article Online
DOI: 10.1039/D4QM00312H

conductivity, other adjustable properties include hydrophilicity or aerophobicity, active site density, electrochemical stability, mechanical properties, and mass transfer efficiency. For example, *Yao* and co-workers [73] reported a novel heterostructure CeO_2/Co_4N electrocatalyst by fabricating oxygen vacancy-rich CeO_2 nanoparticles based on Co_4N nanorod arrays. The synergistic impact of CeO_2/Co_4N can effectively reduce ΔG_{H*} on the catalyst surface, bringing it closer to zero. As a result, at all pH levels, the CeO_2/Co_4N catalyst displayed good HER performance. According to the them, improved HER electrocatlytic activity can be attributed to the synergistic interaction between oxygen-vacancy rich CeO_2 and Co_4N. In addition, *Dhandapani et. al.* [74] used a two-step hydrothermal process to develop a new 2D Mott-Schottky bifunctional electrocatalyst NiFe-LDH/CuS on copper foam. According to them, the enhanced HER activity of NiFe-LDH/CuS/Cu could is ascribed to a synergistic interaction between NiFe-LDH and CuS/Cu. Impressively, this electrode only requires an overpotential of 28 mV to achieve a current density of 10 mA cm^{-2}. Moreover, the fabricated electrode can act as both a cathode and anode catalyst in an electrolysis cell for the overall water splitting. The cell potential of 1.55 V vs RHE to deliver 20 mA cm^{-2} and is capable of withstading in alkaline media for up to 25 hours.

3.2.2 Effects of Mott-Schottky heterojunction on the hydrogen adsorption Gibbs Free Energy

The initial reactant adsorption, subsequent generation of reaction intermediates and the ultimate desorption process, can be used to determine that the electrocatalytic process involving both the HER and OER proceeds. Based on the Sabatier principle [53], a crucial descriptor for HER is ΔG_{H*} [75]. H* adsorbed on the catalyst's surface will be challenging if $|\Delta G_{H*}|$ is too high, however, if the value is too low, the adsorbed H* will hardly desorb to produce H_2(g) [75, 76]. The adsorption energy of H* should be minimal for the ideal catalyst. As a result, the catalysts' chemisorption and desorption

View Article Online
DOI: 10.1039/D4QM00312H

free energies must be adjusted to increase activity. The current density and hydrogen adsorption Gibbs free energy (ΔG_{H*}) always have a volcano-like correlation. The Volcano plot (Figure 4a) shows that noble-metal electrocatalysts with near-zero ΔG_{H*} can be found at the volcano's peak [77]. According to the Sabatier principle, catalysts with high catalytic activity have zero ΔG_{H*} [78, 79]. DFT simulations can elucidate the catalytic process and analyze binding and formation energies, as well as ΔG_{H*}. The formation of a Mott-Schottky junction have been extensively investigated in order to improve the chemisorption and desorption behaviors of catalysts and improve their intrinsic activity towards electrocatalytic reactions. For instance, *Xu et. al*. [76] fabricated Ni-Mo_2C/NC, a Mott-Schottky array catalyst. Figure 4b-d show the optimized models for H* adsorption on the NC, Mo_2C/NC, and Ni-Mo_2C/NC. Figure 4e displays the computed values of $|\Delta G_{H*}|$ for NC, Mo_2C/NC, and Ni-Mo_2C/NC, which were 0.438 eV, 0.134 eV, and 0.052 eV, respectively. The trends of catalytic activity is Ni-Mo_2C/NC > Mo_2C/NC > NC. This demonstrates that the Ni dopant in the Mo_2C/NC lattice can greatly reduce ΔG_{H*} by improving the inherent electronic structure of Mo_2C/NC. In addition, *Luu et al*. [80] developed a Mott-Schottky catalyst, MoS_2/CoS_2, that was grown on conductive CC substrate. Figure 4f demonstrates that the Mo and S sites for MoS_2 have ΔG_{H*} values of –0.32 and 0.59 eV, respectively, which are deviates far from the optimal value 0 eV. The Co(5fld) site's positive ΔG_{H*} values (0.20 eV) show that the binding energy of the H intermediate is too weak, making it difficult for H intermediates to adsorb or desorb on these sites. This slows down the HER kinetics (Figure 4g). The Mott-Schottky effect can optimazed adsorption of H intermediates, and further improving HER kinetics and electrochemica performance. This is corroborated by the optimal ΔG_{H*} values of the Mo (–0.27 eV) and S (0.51 eV) sites ascribed to the MoS_2 component, and the Co (–0.02 eV) and S (–0.09 eV) sites ascribed to the CoS_2 component for the MoS_2/CoS_2 heterojunction (Figure 4h).

3.2.3 Effects of Mott-Schottky heterojunction on the d-band Center and Fermi Level

The ΔG_{H^*} value only represents the current state of the surface electron structure. The d-band center (E_d) is important because the interaction between an adsorbate state and the metal d states is vital for the interaction energy, which is required to properly understand the H* intrinsic surface adsorption capacity, which is directly linked to the d-orbital energy levels [81]. According to the d-band model, because the metal's sp bands are broad and unorganized and the d bands are narrow, moderate changes in the environment might have a major effect on the d states and their interactions with the adsorbate states. As the E_d shifts, the vacant antibonding states will shift up or down [82]. Adsorption of H* on metal catalyst surfaces results in the formation of the metal-hydrogen bond. The H* orbital interacts with the metal d-orbital, creating a partially filled anti-bonding orbital with high energy and a fully filled bonding orbital with low energy. The anti-bonding orbital occupancy impacts the metal-hydrogen bonding strength [83, 84]. A lower anti-bonding orbital occupancy correlates with higher bonding strength. The $E_{F,\,m}$ and the location of the E_d also affect the strength of the metal-hydrogen bond. When the metal's anti-bonding orbital is greater, H* adsorption is stronger, reducing occupancy as the Fermi level (E_F) approaches the E_d. Heterostructure interface engineering is a powerful method for changing the surface electron structure and E_d, resulting in a catalyst with the highest adsorption strength feasible. For example, *Xu* and co-works fabricated Mott-Schottky heterojunction catalyst $NiSe_2/MoSe_2$[36]. Obviously, the Mott-Schottky effect causes the E_d of $NiSe_2$ and $NiSe_2/MoSe_2$ to deviate from the E_F, as demonstrated by their respective E_d values of –2.38 and –2.67 eV. E_d's downward shift allows more electrons to reach the antibonding state, lowering H adsorption and encouraging desorption (Figure 5a). According to the authors, the Mott-Schottky heterojunction can improve the E_d and change the electronic structure, hence promoting HER. Similarly, *Li* and his co-workers [85] reported the fabrication of $MoS_2@Co_3S_4$/NC heterostructure catalyst. Figure 5b

View Article Online
DOI: 10.1039/D4QM00312H

indicates that the HER activity at the heterojunction is accelerated due to a lower H adsorption energy and a weaker contact between the catalyst surface and the adsorbed H intermediates, as estimated by the density of states (DOS) calculation. The Ed of MoS_2@Co_3S_4/NC and MoS_2 relative to E_f were found to be –1.77 and –1.67 eV, respectively. The *Zhang* group [86] reported a Mott−Schottky electrocatalyst Ni/WO_3 with a hedgehog-like nanostructure decorated on Ni foam. The E_d of Ni in Ni/WO_3 could be reduced by electron transport from Ni to WO_3 across the nanointerface, as demonstrated by theoretical calculations and experimental analysis. This results in a moderate H binding strength with small $|\Delta G_{H*}|$ value of 0.097 eV, which promotes HER kinetics (Figure 5c).

3.2.4 Effects of Mott–Schottky heterojunction on the electronic distribution and transport

The electrocatalytic activity of catalysts depends on their atomic configurations and surface electronic structure [87]. Modulating the catalyst's surface charge distribution through creative structural design is critical for improving catalytic performance. To improve electrocatalytic performance, the integrated electric field at the Mott-Schottky junction allows electron transfer at the interface, resulting in surface charge redistribution. This is a powful method for modulating charge transport between the catalyst's surface and the reaction intermediate [88, 89], leading to the exceptional electrocatalytic activity. For example, *Peng et. al.* [90] constructed a conventional Ru-$WO_{2.72}$ Mott-Schottky heterojunction by painting and reducing a small number of Ru species on the $WO_{2.72}$ substrate. At the Ru-$WO_{2.72}$ heterointerface, both theoretical and experimental experiments showed charge density redistribution and the formation of an interfacial electric field (Figure 5d). This resulted in a significant increase in electron concentration at the interface, which improved H* sorption and HER performance. Furthermore, Ru decoration significantly enhances electron DOS at the Fermi level (Figure 5e), revealing electron redistribution within the Ru-$WO_{2.72}$ composite

View Article Online
DOI: 10.1039/D4QM00312H

according to charge density distributions of $WO_{2.72}$ and Ru-$WO_{2.72}$. *Qiao et al.* [91] developed a 1D/3D trepang-like porous N-modified carbon-confined bimetal carbide electrocatalyst including metal cobalt nanoparticles ($Co_6Mo_6C_2$/Co@NC). As seen in the left TEM images in Figure 8f, the hollow channel structure of 1D CNTs allows for control of the local electron environment and enhanced charge transfer. In middle section of the TEM image, the dual Mott-Schottky interfaces Co||NC and $Co_6Mo_6C_2$||NC can activate electric fields which promote electron transport, providing three possible electron transfer highways: Co → NC, NC → $Co_6Mo_6C_2$ or Mo_2C, and Co → NC → $Co_6Mo_6C_2$ or Mo_2C. These electron transfer paths facilitate faster electron transmission across the carbon matrix, allowing for efficient regulation of the electronic density and structure of the $Co_6Mo_6C_2$/Co@NC active sites. Despite, the Mott-Schottky effect's charge redistribution happens at the metal/semiconductor interface can also facilitate the HER electrocatalytic reactions.

3.2.5 Effect of doping and morphology on the performance of Mott-Schottky electrocatalysts

Doping endows the electrocatalysts with better catalytic activity by modulating the charge transfer process and/or electronic structure. The electronic structure is adjusted by doping with anions, which further increases the number of active sites and improves the electrical conductivity. In order to understand the significance of transition metal element doping, Tang and co-workers [92] designed design Mo-doped Mott-Schottky heterostructure Mo-NiCoP@MXene for high efficient HER. The HER mechanisms in Mo-NiCoP@MXene alkaline electrolytes was established (Figure 6a). DFT calculation reveals that the ΔG_{H^*} decreases after introduction of Mo resulting in reduced overpotentials and improved catalytic activity (Figure 6b). Meanwhile, the Mo–NiCoP@MXene are more suitable for the adsorption of H_2O molecules, which makes it more favorable to start the subsequent reaction (Figure 6c). Additionally, in order to improve the catalytic activity, oxygen

View Article Online
DOI: 10.1039/D4QM00312H

defects have also been used to adjust the surface electronic configuration. Additionally, researches show that oxygen vacancies can immensely regulate the surface electronic configuration and optimize the adsorption energies of the reaction intermediates, then facilitated charge transfer and grately boosted intrinsic activity. For example, Xu et al.[93] have produced a typical Mott-Schottky electrocatalyst by immobilizing Ni/CeO_2 hetero-nanoparticles onto N-doped carbon nanofibers (Ni/CeO_2@N-CNFs). Compared with Ni@N-CNFs and CeO_2@N-CNFs, Ni/CeO_2@N-CNFs with rich oxygen vacancies show superior catalytic activities in alkaline electrolyte. Surface morphology design is one of the essential strategies to improve catalysts' surface performance[94]. Recently, Mott-Schottky nanocatalysts such as nanoparticles[95], nanosheets[39], nanowires[96], hollow microspheres[97] as well as nanotubes/nanowire coupled[98] and porous structures[99] have been developed. Generally, during the catalytic reaction, the effect of electrochemical active surface area on catalytic activity is greater than that of physical surface area. However, it is difficult to evaluate the intrinsic activity of the electrocatalysts since the geometric area of active materials can't be accurately determined. In this review, we mostly focus on the progress of Mott-Schottky junction electrocatalysts for pH universal hydrogen evolution reaction. Recently, excellent syntheses and electrochemical application of Mott-Schottky catalysts for pH universal hydrogen evolution reaction have been made (Table 1).

Table 1. Comparison of Mott-Schottky electrocatalysts for HER in various pH values.

Catalysts	Electrolytes	η_{10} [mV]	Tafel Slope [mV dec^{-1}]	References
Ru/CeO_2	1 M KOH	55,	43.3,	*J. Colloid Interf. Sci.*, 652 (2023) 653-62.
	0.5 M H_2SO_4	80	43.3	
	neutral media	120	53.3	

Ru@N-CNFs	1 M KOH	17	31.8	*Small*, 19 (2023) 2206781.
	0.5 M H_2SO_4	16	28.5	
Ru@NCN	1 M KOH	36	37	*J. Mater. Chem. A*., 9 (2021) 13958-66.
	0.5 M H_2SO_4	49	41	
	neutral media	76	54	
V_o-CeO_2/Co_4N	1 M KOH	30	66	*Appl. Cata. B.*, 277 (2020) 119282.
	0.5 M H_2SO_4	33	65	
	neutral media	75	112	
Co_2P/Co_4N	1 M KOH	53	50	*Chem. Eng. J.*, 454 (2023) 140230.
	0.5 M H_2SO_4	32	38	
	neutral media	19	26	
Mo_5N_6-MoS_2/HCNRs	1 M KOH	53	37.9	*Small*, 18 (2022) 2201137
	0.5 M H_2SO_4	57	38.4	
	neutral media	59	43.5	
WS_2/CoS_2/CC	1 M KOH	122	93	*ACS Sustainable Chem. Eng.*, 8 (2020) 4474-4480.
	0.5 M H_2SO_4	146	64	
	neutral media	175	81	
Co/Co_2P@C	1 M KOH	158	64.42	*J. Colloid Interf. Sci.*, 565 (2020) 513-522
	0.5 M H_2SO_4	192	56.35	
Ru@NCN	1 M KOH	36	37	*J. Mater. Chem. A*, 9 (2021) 13958-13966.
	0.5 M H_2SO_4	49	41	
	neutral media	76	54	
Mo-MoS_2 MSH	1 M KOH	138	90.2	*Nano Energy*, 101 (2022) 107563.

	0.5 M H_2SO_4	91	61.9	
	neutral media	128	74.5	
NiCo-nitrides/	1 M KOH	71	58	
$NiCo_2O_4$/GF	0.5 M H_2SO_4	432	68	*Adv. Sci.*, 6 (2019) 1801829
	neutral media	418	78	

4. Mott–Schottky catalysts for pH universal HER

Metal oxide-based materials have recently demonstrated great potential as HER catalysts because to their superior structural and compositional flexibility [100]. Noble metallic catalysts also exhibit improved reaction kinetics because of their high density of electronic states around the Fermi level and huge active surface area [101]. As previously stated, the Mott-Schottky heterojunction construct can change electrical topologies, give a variety of interfaces, and improve charge transfer, all of which considerably boost the activity of hydrogen evolution [102]. Thus, constructing Mott-Schottky with precious metal/metal oxide can improve electrocatalytic efficiency even more, allowing pH universal HER to be optimized. For example, *Chen* and coworkers [103] developed a Ru/CeO_2 Mott-Schottky catalyst by simply adding a little amount of Ru on the CeO_2 substrate (Figure 7a-h). The HRTEM image (Figure 7b) depicts that the heterostructure between Ru and CeO_2 is formed by a series of lattice stripes representing CeO_2 and Ru nanoparticles. Ru and CeO_2 had work functions of 4.02 eV and 6.18 eV, respectively. Electrons transferred from Ru to CeO_2 after Ru deposition on the CeO_2 surface, reduced the Ru/CeO_2 work function to 4.51 (Figure 7c). Visualized $\Delta\rho$ of Ru/CeO_2 (Figure 7d) revealed a positive charge at the Ru interface and a negative charge on the CeO_2 surface. This implies that electrons transferred from Ru to CeO_2 at the interface, and the BEF can have a significant impact on charge redistribution, allowing for the optimal adsorption energy of hydrogen intermediates

View Article Online
DOI: 10.1039/D4QM00312H

at the active site. Ru/CeO_2 also has more efficient water molecule adsorption and H_2 reduction, mainly attributing to the interlayer electron control of the two materials' Mott-Schottky heterojunction. Figure 7e shows that the estimated ΔG_{H^*} values for Ru/CeO_2, CeO_2 (111), and Ru (101) are –0.28, 1.5, and –0.34 eV. Ru/CeO_2 exhibits ΔG_{H^*} values closer to zero, indicating increased HER capacity. Ru/CeO_2 thus achieved highly efficient pH universal HER property with a Tafel slope of 43.3, 43.3, and 53.3 mV dec^{-1}, and achieves the criterion current density of 10 mA cm^{-2} at overpotentials of 55, 80, and 120 mV in alkaline, acidic, and neutral media, respectively, due to the Mott-Schottky effect and charges redistribution at the interface (Figure 7f-h). Furthermore, Ru/CeO_2 demonstrated good HER durability across a wide pH range, with stability lasting 20 hours at 20 mA cm^{-2} and minimal loss after 5000 cycles. In addition, *Wang et al*. [104] developed N, P-codoped graphene nanocomposites Ru-RuO_2@NPC with Ru-RuO_2 Mott-Schottky heterojunctions (Figure 8a-i). The HRTEM image (Figure 8b) demonstrates that the heterostructure between Ru and RuO_2 is formed by stripes of Ru nanoparticles and RuO_2. Charge transfer from electronegative metal Ru to neighboring O and Ru^{4+} sites enhance the electron density of O on the RuO_2 surface for the heterojunction catalyst (Figure 8c). Interfacial interactions between Ru and RuO_2 in the Mott-Schottky heterostructure are likely to influence the adsorption of major catalytic intermediates and, as a result, electrocatalytic activity during the reaction. Figure 8d exhibits an HER diagram indicating H_2O adsorption and dissociation, as well as H adsorption from catalyst surfaces. When compared to pristine RuO_2, the computed DOS reveals that the heterostructure has metallic features with a zero-band gap and Ru d-states that are nearer to the E_F (Figure 8e). The heterojunction's d band center (E_d = –3.28 V) is located between the metal Ru (E_d = –3.10 V) and RuO_2 (E_d = –3.33 V) alone. This indicates that the development of a Mott-Schottky heterojunction Ru-RuO_2 reduces the adsorption of critical reaction intermediates while potentially increasing catalytic performance when compared to Ru metal alone. DFT simulations

showed that the bare Ru and RuO_2 lattices exhibited comparatively high Gibbs free energy (ΔG_{H^*}) values of –0.33 eV and 0.12 eV, respectively. However, for the Ru-RuO_2 heterojunction, this value reduced considerably to only –0.05 eV (Figure 8f), and significantly improved HER performance can be understanded [105]. This shows that the development of a Ru-RuO_2 heterojunction promoted H adsorption/desorption [106]. Thus, in acidic, neutral, and alkaline solution, as shown in Figure 8g-i, Ru-RuO_2@NPC demonstrates remarkable activity and no evident decrease of the current at the fixed working potential of –100 mV for more than 10 hours, indicating its strong HER stability at all pH values. Similarly, *Zhou et. al*. [107] synthesized Ru nanoclusters grown in situ on N-doped carbon nanofibers (Ru@N-CNFs) via a "phenolic resin-bridged" approach and employed in HER at all values (Figure 9a-h). The resultant electrocatalyst revealed exceptional HER performance. The work function difference between Ru (4.71 eV) and N-CNFs (4.87 eV) fulfill the requirements for the formation of a Schottky barrier [108]. After contact, charges from metal Ru will flow naturally to N-CNFs until the E_F are matched. This results in the creation of a Mott-Schottky heterojunction (Figure 9b), which generates an orientated electron flow and an internal electric field (Figure 9c), accelerating the electrocatalytic HER process. The charge density difference plot of the Schottky heterostructure catalyst Ru@NC (Figure 9d) supports the electrons flow naturally from metallic Ru to N-doped carbon support. DOS confirms rapid charge transfer capability for Schottky heterojunctions during HER catalysis, indicating that the E_d of Ru sites in the Ru@NC heterojunction is nearer to the E_F than in pure Ru. The Ru@NC heterostructure has a ΔG_{H^*} value of –0.11 eV, much lower than that of pure Ru (–0.39 eV), as demonstrated in the ΔG_{H^*} graphs (Figure 9e). Ru@N-CNFs exhibit pH-universal HER activity in acidic and alkaline electrolytes, with small overpotentials of 16 and 17 mV at 10 mA cm^{-2} as well as low Tafel slopes of 31.8 and 28.5 mV dec^{-1} (Figure 9g, h). Recently, Sarkar et. al. [109] developed a one-step pyrolysis process to decorate ultrafine Ru nanoparticles in situ on a hollow

View Article Online
DOI: 10.1039/D4QM00312H

N-doped carbon nanocage (Ru@NCN) as a first-class HER catalyst. Ru/N doped carbon exhibits the Mott-Schottky effect, which promotes electron transfer at the interface. Ru@NCN only needed overpotentials of 36, 49, and 76 mV in alkaline, acidic, and neutral environments, with Tafel slopes of 37, 41, and 43 mV dec^{-1}, respectively. This enabled the material to achieve 10 mA cm^{-2}. Metal nitrides have gained a lot of attention due to their remarkable catalytic activity in a range of energy-related processes [110]. Because of the integrated electric field, the Mott-Schottky effect has been regarded as an effective approach to achieve high electrocatalytic activity. For instance, *Yao et. al.* [73] put forward a heterostructure CeO_2/Co_4N catalyst，in which the CeO_2 nanoparticles with lots of oxygen vacancies loaded on Co_4N nanorod arrays (Figure 10a-j). The TEM and HRTEM images demonstrate the successful construction of the Mott-Schottky heterojunction CeO_2/Co_4N, as illustrated in Figures 10b-c. Figures 10d-e show the theory models of DFT calculations for Co_4N and Vo-CeO_2/Co_4N, which suggest that improved HER performance can be ascribed to the synergistic interaction of CeO_2 and Co_4N. According to DFT calculations, the H_2O adsorption free energies of V_o-CeO_2/Co_4N on the CeO_2 site (V_o-Ce) and Co_4N on the Co_4 site are –0.78 eV and –0.16 eV, respectively (Figure 10f). These results show that the adsorption of H_2O on the Vo-CeO_2 surface is substantially more than on the Co_4N surface. Furthermore, as shown in Figure 10g, the computed water dissociation barrier for CeO_2/Co_4N and Co_4N demonstrates that the water dissociation barrier on CeO_2/Co_4N is less than that on Co_4N [83, 111]. As a result, by accelerating water adsorption and dissociation of the Volmer step in the HER process, V_o-CeO_2 can improve catalytic HER ability of Co_4N. Concurrently, the charge of Co surrounding V_o-Ce sites is higher than that of Co_4N, indicating that H adsorption is inhibited due to positively charged hydrogen atoms. According to the computed d-band density of states (d-DOS) study of Co in Co_4N and V_o-CeO_2/Co_4N, V_o-CeO_2 will affect the electronic distribution of Co_4N and shift the E_d of Co atoms further away from the E_F as shown in

View Article Online
DOI: 10.1039/D4QM00312H

Figure 10h. V_o-CeO_2/Co_4N exhibits higher thermos-neutral ΔG_{H^*} compared to Co_4N (Figure 10i), indicating superior HER performance. The ideal V_o-CeO_2/Co_4N showed good HER performance in 1.0 M KOH, 0.5 M H_2SO_4, and neutral electrolytes, with overpotentials of 30, 33, and 75 mV, respectively, attaining 10 mA cm^{-2} (Figure 10j-l). Since phosphorus may efficiently interact with protons during an electrochemical process and act as a Lewis base to collect electrons from transition metals, transition metal phosphides exhibit excellent HER activity [112]. However, a recent study shows that some nitrides, such as Mo_5N_6 and Co_4N, have good metal features [113, 114]. Thus, constructing a Mott-Schottky heterojunction using mixed nitrides and phosphides could be an excellent way to improve HER catalytic performance. As a result, we demonstrate a hybrid Mott-Schottky electrocatalyst constituted by both of n-type semiconducting Co_2P and metallic Co_4N (Figure 11a-i) [24]. Figure 11a depicts the Co_2P and Co_4N structural models. Energy band diagrams revealed that the semiconducting Co_2P (4.8 eV) had a significantly lower work function compared to the significantly greater 5.35 eV work function of Co_4N. As a result, the Co_2P/Co_4N heterojunction formed an inherent electric field, which accelerated electron transport from the semiconductor Co_2P side to the metallic Co_4N side until equilibrium Fermi levels were achieved (Figure 11b-c). The XPS investigation and DFT calculation findings confirmed the aforementioned charge redistribution between the Co_4N and Co_2P contacts. The electrons at the Co_2P/Co_4N interface have been reallocated, as evidenced by blue and yellow patches (Figure 11d). The Mott-Schottky heterojunction occurs at the contact metallic Co_4N and the semiconductor Co_2P, confirming metallic nature of Co_4N. DFT calculations reveal that the DOS spans the E_F. Following subsequent calculations, the density of Co-3d was found to exhibit substantial density states near the E_F, indicating that the electrical conductivity of Co_2P/Co_4N was increased (Figure 11e). The electrocatalysts have advantages for water adsorption, as evidenced by the negative water adsorption energies at the Co_4N, Co_2P, and

View Article Online
DOI: 10.1039/D4QM00312H

Co_2P/Co_4N interfaces of the three samples, Co_2P/Co_4N owns the smallest water adsorption value [115]. The HER process in an alkaline media was determined by the water dissociation [116], whereas H adsorption affected the HER reaction rate in an acidic environment [117]. Figure 11f shows that the Co_2P/Co_4N has a lower hydrogen adsorption energy (–0.36 eV) than Co_2P and Co_4N (–0.84 eV and –1.19 eV), respectively. The Co_2P/Co_4N Mott-Schottky heterojunction enhances H* adsorption kinetics, as evidenced by the moderate ΔG_{H^*} ($|\Delta G_{H^*}| = 0$) available for H_2 evolution [118]. Thus, the extraordinary Co_2P/Co_4N HER activity is due to the mutually elevated ΔG_{H^*} and water dissociation, which permit both the Heyrovsky and Volmer phases of the HER process [73]. Theoretical and experimental results were consistent, with the Co_2P/Co_4N Mott-Schottky heterojunction catalyst demonstrating super HER performance. Achieving 10 mA per square centimeter current densities in 0.5 M H_2SO_4, 1.0 M KOH, and neutral electrolytes required only 32, 53, and 19 mV of overpotential (Figure 11g-i). Chalcogenides have high activity, exceptional stability, and are free of precious metals, making them attractive HER catalysts [119]. Materials containing molybdenum sulfide, such as MoS_2, have shown potential for electrochemical hydrogen production. MoS_2 for HER catalysis has made tremendous advances in recent years, several of which have been previously reviewed [120, 121]. Chalcogenides can thus participate in HER effectively thanks to the Mott-Schottky effect, which increases their catalytic activity. Recently, *Pi et al.* [122] developed a Mott-Schottky heterojunction catalyst Mo_5N_6-MoS_2/HCNRs by thermal nitridation of 2H-MoS_2 nanosheets on HCNRs, which are generated by thermal assisted nitriding of 2H-MoS_2/PPy in NH_3 (Figure 121a-h). The work functions of Mo_5N_6 and 2H-MoS_2 are 5.83 eV and 7.62 eV, respectively. Figure 12b depicts the plotted energy band diagrams of Mo_5N_6 and 2H-MoS_2 before and after contact. According to the XPS results, the system's internal electric field leads valence electrons to flow from 2H-MoS_2 to Mo_5N_6 until equilibrium is reached [89]. According to the researchers, the intrinsic electric field and electron

View Article Online
DOI: 10.1039/D4QM00312H

redistribution at the interface of 2H-MoS_2 and Mo_5N_6 significantly activate the inert MoS_2 basal planes, increasing MoS_2 electrocatalytic activity and facilitating Mo_5N_6 water dissociation. The wavelet transforms intensity optimum for Mo-Mo bonding in Mo_5N_6-MoS_2/HCNRs and 2H-MoS_2/HCNRs is around 10 Å and 9.4 Å, respectively, as shown in Figure 12c. This shows that the coordination of Mo-S is often unsaturated because of the synthesis of Mo_5N_6, which results in enhanced unsaturated sites [123] and defects, which enable robust catalytic activity of HER. The calculated E_d values of Mo_5N_6-MoS_2 and 2H-MoS_2 (Figure 12d) relative to E_F are −1.75 and −0.12eV, respectively [124]. The E_d of the Mo_5N_6-MoS_2 heterojunction is substantially far away from the E_F, which indicates weaker interactions between the hydrogen adsorbate and catalytic surface, as well as lower antibonding energy states that enhance HER kinetics. As shown in Figure 12e, the addition of Mo_5N_6 generates active sites for hydroxyl adsorption, facilitating the dissociation of HO-H bonds and the formation of hydrogen intermediates. As a result, the activation barrier for H_2O dissociation at the Mo_5N_6-MoS_2 interface is much lower, measuring 0.18 eV. The ΔG_{H^*} of the Mo_5N_6-MoS_2 heterojunction coincides with the S sites on the edge plane of 2H-MoS_2 at –0.06 eV, which is amazing. This suggests that coupling with Mo_5N_6 completely activates the basal plane sites of 2H-MoS_2, resulting in an in-plane Mo_5N_6-MoS_2 heterojunction. Figure 12f shows that effective water adsorption occurs after combining with Mo_5N_6, with the H_2O adsorption energy at the Mo_5N_6-MoS_2 heterojunction (–0.85 eV) being 6 times less than that of the MoS_2 basal plane (–0.14 eV). The Mott-Schottky-type Mo_5N_6-MoS_2 heterostructure produces better HER kinetics, which is helpful for electron shift, hydrogenolysis energy, and H_2O adsorption/dissociation. The Mo_5N_6-MoS_2/HCNRs Mott-Schottky catalyst has excellent pH-universal HER performances (Figure 12g-i), requiring extremely low overpotentials of 57, 53, and 59 mV at 10 mA cm^{-2} in acidic, alkaline, and neutral solutions with Tafel slopes of 38.4, 37.9, and 43.5 mV dec^{-1}, respectively. This is owing to the

View Article Online
DOI: 10.1039/D4QM00312H

combined action of in-plane Mo_5N_6-MoS_2 and underlying HCNRs.

Similarly, *Wu et al* and his co-workers [125] Wu et al. and colleagues [109] proposed a unique Mott-Schottky nanosheet array catalyst supported on carbon cloth (WS_2/CoS_2/CC) with excellent HER activity in all pH values (Figure 13a–f). When S bridges WS_2 and CoS_2 in the WS_2/CoS_2/CC catalyst, a WS_2/CoS_2 heterojunction is formed. A W-S-Co bond may develop at the contact (see Figure 13a) [124, 126]. Figure 13b shows that WS_2 and CoS_2 have unique work functions (i.e., 5.50 eV and 5.89 eV, respectively) [127, 128]. It is clear that CoS_2 has a higher E_F than WS_2, causing electrons to move from CoS_2 to WS_2 across the interface. This process continues until the E_F equilibrium, at which point the WS_2/CoS_2 electrical modulation occurs. The HRTEM image (Figure 13c) further illustrates the internal heterostructure of WS_2/CoS_2. Excellent HER activities of WS_2/CoS_2/CC with long-term stability in all pH values can be produced by accelerating electron move at the heterointerface, which is made possible by the built-in electric field at the interface due to Mott-Schottky effect. To achieve 10 mA cm^{-2} in 0.5 M H_2SO_4, 1.0 M KOH and 1.0 M phosphate buffer solution (PBS), Figure 13d-f demonstrates that overpotentials of 146, 122, and 175 mV are adequate.

Sun and his co-works [129] developed Mo–MoS_2 Mott–Schottky catalyst for HER in wide pH values by an in situ lithiation method (Figure 13g-k). The mass transfer process can be accelerated by adding nano-Mo to enhance in-place conductivity. According to DFT calculations, Mott-Schottky heterojunctions improve interfacial electron contacts and electron transport from Mo atoms to sulfur sites at active sites, activating the sulfur sites and substantially enhancing HER catalytic activity (Figure 13g). Figure 13h shows that the Mo-2 H-MoS_2 and Mo-1 T-MoS_2 Mott-Schottky heterostructures have higher ΔG_H values (i.e., 0.387 and 0.243 eV, respectively) compared to Mo-2H-MoS_2 (–0.578 eV for S site) and 1T-MoS_2 (–0.434 eV for S site). This shows that introducing

View Article Online
DOI: 10.1039/D4QM00312H

nano-Mo into the MoS_2 lattice can have a significant impact on interfacial electron rearrangement and electron/proton move at sulfur sites, hence improving HER activity. As revealed in Figure 13i-k, the optimal Mo-MoS_2 Mott-Schottky heterostructure catalyst possesses remarkable HER performance and durability across the pH range.

In response to the energy crisis, electrochemical water splitting has been widely concerned as a promising method of hydrogen production. Economic hydrogen production requires the development of cheap catalysts with high perofrmance and long-term stability. When it comes to water electrolysis, Mott-Schottky heterostructure catalysts perform better electrocatalytically with the following advantages: An oriented internal electric field, steady local electrophilic/nucleophilic regions, tunable surface chemisorption energy, spontaneous electron shift across the Schottky interface until the work functions on both sides reach equilibrium and form the new E_F, and a well-connected electronic path at the atomic level. Significant step forward has been achieved in the development and production of Mott-Schottky catalysts in recent years. However, understanding the reaction mechanism and cutting-edge controlled fabrication procedures remains a challenge.

5. Some challenges and future perspectives

5.1. Widening pH with Greater Tolerance

A significant number of currently available pH universal Mott-Schottky electrocatalysts have been studied as alkaline, acidic, and neutral electrolytes in mild pH conditions such as 1 M KOH, 0.5 M H_2SO_4, and 1 M PBS. Nonetheless, in practical industrial operations, electrolyzers must work in rugged environments with concentrations as high as 6-10 M. Tight, close-contact interfaces are essential for optimum interaction and stability; even more important, such interfaces must be chemically and corrosion resistant.

View Article Online
DOI: 10.1039/D4QM00312H

5.2. Scalability over Long Duration

Even though the activity of Mott-Schottky catalysts has increased dramatically, their use in water electrolysis devices has been severely limited due to their poor performance stability and tendency to degrade catalytically. A majority of HER non-noble interfacial catalysts continue to exhibit an average stability of 200-300 hours; very few articles reported stability of up to 1000 hours continuous operations [130, 131] Thus, the most significant criteria for the newly constructed Mott-Schottky electrocatalyst is the long-term stability. Furthermore, a majority of surveys only examine how long performance endures in working environments; very few investigated the reason of performance decline. As a result, significant efforts should be taken to develop feasible approaches to identify the primary causes of activity decline.

5.3. The deep mechanism of synergy effect

Mott-Schottky heterostructure catalysts exhibit excellent catalytic activity, which is often explained by the synergistic effect. However, it should be emphasized that further studies are needed to properly understand the true synergistic effect of different heterostructure catalysts. To understand the real nature of the synergistic effect and how it causes the catalysts to deliver higher catalytic activity, more substantial evidence needs to be obtained. For a more fundamental understanding and intelligent heterostructure catalyst design, combining theory and experiment investigation in electrocatalysis is also crucial.

5.4. Advanced Characterization Techniques and Theoretical Analysis

Research has concentrated on the surface and structure of Mott-Schottky heterostructures. To measure the intermediates at different reaction periods, Ex situ analytical methods like electron

View Article Online
DOI: 10.1039/D4QM00312H

microscopy (TEM and FESEM) and XRD are applied. It remains uncertain which catalytic active areas are critical for catalyst design. In order to fully understand the fundamental concepts, electrical behavior, and interfacial charge transport mechanisms in Mott-Schottky catalysts catalytic processes, along with the real-time multi-step reaction routes, more accurate in-situ/operando characterization is requested. To completely understand the reaction mechanism and pathway, in-situ/in-operando characterization approaches for the Mott-Schottky heterostructure, such as in-situ Raman, differential electrochemical mass spectrometer (DEMS) and X-ray absorption spectroscopy (XAS), must be used [132, 133]. These methods provide a complete analysis of the change in the local electronic structure of the electrocatalysts, as well as the process of capturing reaction intermediates on the electrocatalyst surfaces. Furthermore, the majority of theoretical models (DFT, molecular dynamics, Monte Carlo, etc.) of the electronic structure and charge density differences in the Schottky junction may only predict the general direction of electrochemical activity [134, 135]. Nonetheless, the mechanisms behind heterostructure interfacial electron transport and their inherent interaction with Schottky heterojunctions for electrocatalysis are poorly understood on the molecular, atomic, and electronic levels. Advanced computational methods, such as operando modeling and machine learning-based algorithms [136] can solve these issues and accelerate the development of high-performing catalysts for water electrolysis applications. Academics studying electrochemistry energy conversion and storage certainly with the help of advanced computing device.

5.5. Scaling up and Understanding Economy

Although green hydrogen production yields almost zero emissions, the scale-up framework is undermined by the application of expensive precious metals like platinum as catalysts. Nevertheless, as we all known that these metals are rare, expensive, and noble. Although many heterostructure

View Article Online
DOI: 10.1039/D4QM00312H

catalysts exhibit remarkable performance and meet the requirements of industrial applications. scaling up catalyst synthesis is a significant barrier to the industrial application of electrochemical HER catalysts, and most synthesis processes are limited to laboratory. As a result, one of the key challenges to commercializing Mott-Schottky catalysts is fail to establish an accessible and easily scalable fabrication technology. In consequence, one of the most significant challenges in constructing a commercial water splitting electrolyzer is producing an electrocatalyst that is highly-efficient, affordable, and can be prepared on large scale. All in all, it can be believed that developing well-defined Mott-Schottky catalysts at all pH levels is a pretty prospective and unique approach to designing highly effective catalysts for electrochemical water splitting, and that the fast prograss of electrochemical water electrolysis powered by renewable energy sources will shed light on the future hydrogen economy.

Acknowledgements

This work is finically supported by National Natural Science Foundation of China (Grants No. 52272202, 51972129), Natural Science Foundation of Jiangxi Province (20212BAB201021), Bintuan Science and Technology Program (Grants No. 2020DB002, 2022DB009), and the Shenzhen Science and Technology Innovation Committee (No. JCYJ20200109141412308). M. Humayun and C. Wang would like to acknowledge Prince Sultan University.

References

[1] Zou C, Zhao Q, Zhang G, Xiong B. Energy revolution: From a fossil energy era to a new energy era. Natural Gas Industry B 2016;3:1-11.

[2] Montoya JH, Seitz LC, Chakthranont P, Vojvodic A, Jaramillo TF, Nørskov JK. Materials for solar fuels and chemicals. Nat Mater 2017;16:70-81.

[3] Tuller HL. Solar to fuels conversion technologies: a perspective. Materials for Renewable and Sustainable Energy 2017;6:3.

[4] Lubitz W, Tumas W. Hydrogen: An Overview. Chem Rev 2007;107:3900-3.

[5] Chen B, Humayun M, Li Y, Zhang H, Sun H, Wu Y, et al. Constructing Hierarchical Fluffy CoO–Co_4N@NiFe-LDH Nanorod Arrays for Highly Effective Overall Water Splitting and Urea Electrolysis. ACS Sustainable Chem Eng 2021;9:14180-92.

[6] Schlapbach L, Züttel A. Hydrogen-storage materials for mobile applications. Nature 2001;414:353-8.

[7] Wang Y, Chen M, Li X, Yang Z, Liang T, Zhou Z, et al. Hydrogen production via steam reforming of ethylene glycol over Attapulgite supported nickel catalysts. Int J Hydrogen Energy 2018;43:20438-50.

[8] Han C, Mei B, Zhang Q, Zhang H, Yao P, Song P, et al. Atomic Ru coordinated by channel ammonia in V-doped tungsten bronze for highly efficient hydrogen-evolution reaction. Chinese Journal of Catalysis 2023;51:80-9.

[9] Anantharaj S, Ede SR, Sakthikumar K, Karthick K, Mishra S, Kundu S. Recent Trends and Perspectives in Electrochemical Water Splitting with an Emphasis on Sulfide, Selenide, and Phosphide Catalysts of Fe, Co, and Ni: A Review. ACS Catal 2016;6:8069-97.

[10] Li H, Chen S, Zhang Y, Zhang Q, Jia X, Zhang Q, et al. Systematic design of superaerophobic

View Article Online
DOI: 10.1039/D4QM00312H

nanotube-array electrode comprised of transition-metal sulfides for overall water splitting. Nat Commun 2018;9:2452.

[11] Yu M, Budiyanto E, Tüysüz H. Principles of Water Electrolysis and Recent Progress in Cobalt-, Nickel-, and Iron-Based Oxides for the Oxygen Evolution Reaction. Angewandte Chemie International Edition 2022;61:e202103824.

[12] Symes D, Taylor-Cox C, Holyfield L, Al-Duri B, Dhir A. Feasibility of an oxygen-getter with nickel electrodes in alkaline electrolysers. Materials for Renewable and Sustainable Energy 2014;3:27.

[13] Anantharaj S, Ede SR, Karthick K, Sam Sankar S, Sangeetha K, Karthik PE, et al. Precision and correctness in the evaluation of electrocatalytic water splitting: revisiting activity parameters with a critical assessment. Energy Environ Sci 2018;11:744-71.

[14] Li W, Jiang N, Hu B, Liu X, Song F, Han G, et al. Electrolyzer Design for Flexible Decoupled Water Splitting and Organic Upgrading with Electron Reservoirs. Chem 2018;4:637-49.

[15] You B, Sun Y. Innovative Strategies for Electrocatalytic Water Splitting. Acc Chem Res 2018;51:1571-80.

[16] Walter MG, Warren EL, McKone JR, Boettcher SW, Mi Q, Santori EA, et al. Solar Water Splitting Cells. Chem Rev 2010;110:6446-73.

[17] Yu F, Zhou H, Huang Y, Sun J, Qin F, Bao J, et al. High-performance bifunctional porous non-noble metal phosphide catalyst for overall water splitting. Nat Commun 2018;9:2551.

[18] Cheng N, Stambula S, Wang D, Banis MN, Liu J, Riese A, et al. Platinum single-atom and cluster catalysis of the hydrogen evolution reaction. Nat Commun 2016;7:13638.

[19] Strmcnik D, Lopes PP, Genorio B, Stamenkovic VR, Markovic NM. Design principles for hydrogen evolution reaction catalyst materials. Nano Energy 2016;29:29-36.

View Article Online
DOI: 10.1039/D4QM00312H

[20] Strmcnik D, Uchimura M, Wang C, Subbaraman R, Danilovic N, van der Vliet D, et al. Improving the hydrogen oxidation reaction rate by promotion of hydroxyl adsorption. Nature Chemistry 2013;5:300-6.

[21] Zhang H, Song P, Yao P, Zhang D, Cao J, Gong X, et al. Three-phase-boundary Pt in a self-supported $MoPt_2$-$MoNi_4/Mo_2C$ heterojunction electrocatalyst for highly efficient pH-universal hydrogen evolution reaction. Chem Eng J 2023;470:144375.

[22] Maji M, Dihingia N, Dutta S, Parvin S, Pati SK, Bhattacharyya S. Charge transfer modulated heterointerfaces for hydrogen production at all pH values. J Mater Chem A 2022;10:24927-37.

[23] Kuang P, Tong T, Fan K, Yu J. In Situ Fabrication of Ni–Mo Bimetal Sulfide Hybrid as an Efficient Electrocatalyst for Hydrogen Evolution over a Wide pH Range. ACS Catal 2017;7:6179-87.

[24] Qin M, Chen L, Zhang H, Humayun M, Fu Y, Xu X, et al. Achieving highly efficient pH-universal hydrogen evolution by Mott-Schottky heterojunction of Co_2P/Co_4N. Chem Eng J 2023;454:140230.

[25] Najafi L, Bellani S, Oropesa-Nuñez R, Ansaldo A, Prato M, Del Rio Castillo AE, et al. Doped-$MoSe_2$ Nanoflakes/3d Metal Oxide–Hydr(Oxy)Oxides Hybrid Catalysts for pH-Universal Electrochemical Hydrogen Evolution Reaction. Adv Energy Mater 2018;8:1801764.

[26] Bhowmik T, Kundu MK, Barman S. Palladium Nanoparticle–Graphitic Carbon Nitride Porous Synergistic Catalyst for Hydrogen Evolution/Oxidation Reactions over a Broad Range of pH and Correlation of Its Catalytic Activity with Measured Hydrogen Binding Energy. ACS Catal 2016;6:1929-41.

[27] Wang Q, Zhang Y, Ni W, Zhang Y, Sun T, Zhang J, et al. Free-standing phosphorous-doped molybdenum nitride in 3D carbon nanosheet towards hydrogen evolution at all pH values. Journal of

Energy Chemistry 2020;50:44-51.

View Article Online
DOI: 10.1039/D4QM00312H

[28] Gu M, Jiang L, Zhao S, Wang H, Lin M, Deng X, et al. Deciphering the Space Charge Effect of the p–n Junction between Copper Sulfides and Molybdenum Selenides for Efficient Water Electrolysis in a Wide pH Range. ACS Nano 2022;16:15425-39.

[29] Zhao G, Jiang Y, Dou S-X, Sun W, Pan H. Interface engineering of heterostructured electrocatalysts towards efficient alkaline hydrogen electrocatalysis. Science Bulletin 2021;66:85-96.

[30] Zeng M, Li Y. Recent advances in heterogeneous electrocatalysts for the hydrogen evolution reaction. J Mater Chem A 2015;3:14942-62.

[31] Staszak-Jirkovský J, Malliakas Christos D, Lopes Pietro P, Danilovic N, Kota Subrahmanyam S, Chang K-C, et al. Design of active and stable Co–Mo–Sx chalcogels as pH-universal catalysts for the hydrogen evolution reaction. Nat Mater 2016;15:197-203.

[32] Popczun EJ, McKone JR, Read CG, Biacchi AJ, Wiltrout AM, Lewis NS, et al. Nanostructured Nickel Phosphide as an Electrocatalyst for the Hydrogen Evolution Reaction. J Am Chem Soc 2013;135:9267-70.

[33] Ren B, Gong X, Cao J, Zhang D, Wang Z, Song P, et al. Heterostructured Pt-Ni_3Mo_3N formed via ammonia-containing polyoxometalates for highly efficient electrocatalytic hydrogen evolution in acid medium. Journal of Energy Chemistry 2024;92:698-704.

[34] Wang F, He P, Li Y, Shifa TA, Deng Y, Liu K, et al. Interface Engineered WxC@WS2 Nanostructure for Enhanced Hydrogen Evolution Catalysis. Adv Funct Mater 2017;27:1605802.

[35] Yan H, Tian C, Wang L, Wu A, Meng M, Zhao L, et al. Phosphorus-Modified Tungsten Nitride/Reduced Graphene Oxide as a High-Performance, Non-Noble-Metal Electrocatalyst for the Hydrogen Evolution Reaction. Angewandte Chemie International Edition 2015;54:6325-9.

[36] Xu X, Liao H, Huang L, Chen S, Wang R, Wu S, et al. Surface reconstruction and directed

View Article Online
DOI: 10.1039/D4QM00312H

electron transport in $NiSe_2/MoSe_2$ Mott-Schottky heterojunction catalysts promote urea-assisted water splitting. Appl, Cata, B 2024;341:123312.

[37] Gu C, Zhou G, Yang J, Pang H, Zhang M, Zhao Q, et al. NiS/MoS_2 Mott-Schottky heterojunction-induced local charge redistribution for high-efficiency urea-assisted energy-saving hydrogen production. Chem Eng J 2022;443:136321.

[38] Yun S, Gao Z, Yang T, Sun M, Yang G, Wang K, et al. Constructing $NiSe_2/MoSe_2$ Mott–Schottky Heterojunctions Onto N-doped Brain Coral-Carbon Spheres by Phase Separation Strategies for Advanced Energy Conversion Applications. Adv Funct Mater;n/a:2314226.

[39] Zhang P, Liu Y, Liang T, Ang EH, Zhang X, Ma F, et al. Nitrogen-doped carbon wrapped Co-Mo_2C dual Mott–Schottky nanosheets with large porosity for efficient water electrolysis. Appl, Cata, B 2021;284:119738.

[40] Adán-Más A, Silva TM, Guerlou-Demourgues L, Montemor MF. Application of the Mott-Schottky model to select potentials for EIS studies on electrodes for electrochemical charge storage. Electrochim Acta 2018;289:47-55.

[41] Su H, Zhang K-X, Zhang B, Wang H-H, Yu Q-Y, Li X-H, et al. Activating Cobalt Nanoparticles via the Mott–Schottky Effect in Nitrogen-Rich Carbon Shells for Base-Free Aerobic Oxidation of Alcohols to Esters. J Am Chem Soc 2017;139:811-8.

[42] Tong Y, Liu W, Li C, Liu X, Liu J, Zhang X. A metal/semiconductor contact induced Mott–Schottky junction for enhancing the electrocatalytic activity of water-splitting catalysts. Sustainable Energy & Fuels 2023;7:12-30.

[43] Krishnamachari M, Lenus S, Pradeeswari K, Arun pandian R, Kumar M, Chang J-H, et al. Review of Mott–Schottky-Based Nanoscale Catalysts for Electrochemical Water Splitting. ACS Applied Nano Materials 2023;6:16106-39.

View Article Online
DOI: 10.1039/D4QM00312H

[44] Cheng Y, Jiang SP. Advances in electrocatalysts for oxygen evolution reaction of water electrolysis-from metal oxides to carbon nanotubes. Progress in Natural Science: Materials International 2015;25:545-53.

[45] Wei J, Zhou M, Long A, Xue Y, Liao H, Wei C, et al. Heterostructured Electrocatalysts for Hydrogen Evolution Reaction Under Alkaline Conditions. Nano-Micro Letters 2018;10:75.

[46] Han C, Zhang S, Zhang H, Dong Y, Yao P, Du Y, et al. Metal−support interaction in single-atom electrocatalysts: A perspective of metal oxide supports. eScience 2024:100269.

[47] Kudo A, Miseki Y. Heterogeneous photocatalyst materials for water splitting. Chem Soc Rev 2009;38:253-78.

[48] Nguyen PD, Duong TM, Tran PD. Current progress and challenges in engineering viable artificial leaf for solar water splitting. Journal of Science: Advanced Materials and Devices 2017;2:399-417.

[49] Dobó Z, Palotás ÁB. Impact of the voltage fluctuation of the power supply on the efficiency of alkaline water electrolysis. Int J Hydrogen Energy 2016;41:11849-56.

[50] Jiao Y, Zheng Y, Jaroniec M, Qiao SZ. Design of electrocatalysts for oxygen- and hydrogen-involving energy conversion reactions. Chem Soc Rev 2015;44:2060-86.

[51] You B, Sun Y. Chalcogenide and Phosphide Solid-State Electrocatalysts for Hydrogen Generation. ChemPlusChem 2016;81:1045-55.

[52] Zheng Y, Jiao Y, Vasileff A, Qiao S-Z. The Hydrogen Evolution Reaction in Alkaline Solution: From Theory, Single Crystal Models, to Practical Electrocatalysts. Angewandte Chemie International Edition 2018;57:7568-79.

[53] Kari J, Olsen JP, Jensen K, Badino SF, Krogh KBRM, Borch K, et al. Sabatier Principle for Interfacial (Heterogeneous) Enzyme Catalysis. ACS Catal 2018;8:11966-72.

View Article Online
DOI: 10.1039/D4QM00312H

[54] Medford AJ, Vojvodic A, Hummelshøj JS, Voss J, Abild-Pedersen F, Studt F, et al. From the Sabatier principle to a predictive theory of transition-metal heterogeneous catalysis. J Catal 2015;328:36-42.

[55] Mahmood N, Yao Y, Zhang J-W, Pan L, Zhang X, Zou J-J. Electrocatalysts for Hydrogen Evolution in Alkaline Electrolytes: Mechanisms, Challenges, and Prospective Solutions. Advanced Science 2018;5:1700464.

[56] Fic K, Meller M, Menzel J, Frackowiak E. Around the thermodynamic limitations of supercapacitors operating in aqueous electrolytes. Electrochim Acta 2016;206:496-503.

[57] Zahra R, Pervaiz E, Yang M, Rabi O, Saleem Z, Ali M, et al. A review on nickel cobalt sulphide and their hybrids: Earth abundant, pH stable electro-catalyst for hydrogen evolution reaction. Int J Hydrogen Energy 2020;45:24518-43.

[58] Herraiz-Cardona I, Ortega E, Antón JG, Pérez-Herranz V. Assessment of the roughness factor effect and the intrinsic catalytic activity for hydrogen evolution reaction on Ni-based electrodeposits. Int J Hydrogen Energy 2011;36:9428-38.

[59] Wei C, Xu ZJ. The Comprehensive Understanding of as an Evaluation Parameter for Electrochemical Water Splitting. Small Methods 2018;2:1800168.

[60] Periassamy M, Krishnaswamy PR. Corrosion rate and tafel slopes from polarization curves. Journal of Electroanalytical Chemistry and Interfacial Electrochemistry 1975;61:349-52.

[61] Kucernak AR, Zalitis C. General Models for the Electrochemical Hydrogen Oxidation and Hydrogen Evolution Reactions: Theoretical Derivation and Experimental Results under Near Mass-Transport Free Conditions. J Phys Chem C 2016;120:10721-45.

[62] Bandal H, Reddy KK, Chaugule A, Kim H. Iron-based heterogeneous catalysts for oxygen evolution reaction; change in perspective from activity promoter to active catalyst. J Power Sources

2018;395:106-27.

View Article Online
DOI: 10.1039/D4QM00312H

[63] Park S, Schultz T, Shin D, Mutz N, Aljarb A, Kang HS, et al. The Schottky–Mott Rule Expanded for Two-Dimensional Semiconductors: Influence of Substrate Dielectric Screening. ACS Nano 2021;15:14794-803.

[64] Wang J, Wang S-Q. Surface energy and work function of fcc and bcc crystals: Density functional study. Surf Sci 2014;630:216-24.

[65] Zhang Z, Yates JT, Jr. Band Bending in Semiconductors: Chemical and Physical Consequences at Surfaces and Interfaces. Chem Rev 2012;112:5520-51.

[66] Liu J, Yang X, Si F, Zhao B, Xi X, Wang L, et al. Interfacial component coupling effects towards precise heterostructure design for efficient electrocatalytic water splitting. Nano Energy 2022;103:107753.

[67] Yang Y, Luo M, Zhang W, Sun Y, Chen X, Guo S. Metal Surface and Interface Energy Electrocatalysis: Fundamentals, Performance Engineering, and Opportunities. Chem 2018;4:2054-83.

[68] Du Y, Li B, Xu G, Wang L. Recent advances in interface engineering strategy for highly-efficient electrocatalytic water splitting. InfoMat 2023;5:e12377.

[69] Zhai L, She X, Zhuang L, Li Y, Ding R, Guo X, et al. Modulating Built-In Electric Field via Variable Oxygen Affinity for Robust Hydrogen Evolution Reaction in Neutral Media. Angewandte Chemie International Edition 2022;61:e202116057.

[70] Xu Q, Zhang J, Zhang H, Zhang L, Chen L, Hu Y, et al. Atomic heterointerface engineering overcomes the activity limitation of electrocatalysts and promises highly-efficient alkaline water splitting. Energy Environ Sci 2021;14:5228-59.

[71] Prabhu P, Jose V, Lee J-M. Design Strategies for Development of TMD-Based Heterostructures in Electrochemical Energy Systems. Matter 2020;2:526-53.

View Article Online
DOI: 10.1039/D4QM00312H

[72] Zhou M, Xu Y, Lei Y. Heterogeneous nanostructure array for electrochemical energy conversion and storage. Nano Today 2018;20:33-57.

[73] Yao N, Meng R, Wu F, Fan Z, Cheng G, Luo W. Oxygen-Vacancy-Induced CeO_2/Co_4N heterostructures toward enhanced pH-Universal hydrogen evolution reactions. Appl, Cata, B 2020;277:119282.

[74] N Dhandapani H, Karmakar A, Selvasundarasekar SS, Kumaravel S, Nagappan S, Madhu R, et al. Modulating the Surface Electronic Structure of Active Ni Sites by Engineering Hierarchical NiFe-LDH/CuS over Cu Foam as an Efficient Electrocatalyst for Water Splitting. Inorg Chem 2022;61:21055-66.

[75] Seo MH, Park HW, Lee DU, Park MG, Chen Z. Design of Highly Active Perovskite Oxides for Oxygen Evolution Reaction by Combining Experimental and ab Initio Studies. ACS Catal 2015;5:4337-44.

[76] Xu Z, Jin S, Seo MH, Wang X. Hierarchical Ni-Mo2C/N-doped carbon Mott-Schottky array for water electrolysis. Appl, Cata, B 2021;292:120168.

[77] Seh ZW, Kibsgaard J, Dickens CF, Chorkendorff I, Nørskov JK, Jaramillo TF. Combining theory and experiment in electrocatalysis: Insights into materials design. Science 2017;355:eaad4998.

[78] Wang C, Wang X, Zhang T, Qian P, Lookman T, Su Y. A descriptor for the design of 2D MXene hydrogen evolution reaction electrocatalysts. J Mater Chem A 2022;10:18195-205.

[79] Wang L, Zhang X, Meng W, Liu Y, Dai X, Liu G. A topological quantum catalyst: the case of two-dimensional traversing nodal line states associated with high catalytic performance for the hydrogen evolution reaction. J Mater Chem A 2021;9:22453-61.

[80] Luyen Doan TL, Nguyen DC, Kang K, Ponnusamy A, Eya HI, Dzade NY, et al. Advanced Mott-Schottky heterojunction of semi-conductive MoS_2 nanoparticles/metallic CoS_2 nanotubes as an

View Article Online
DOI: 10.1039/D4QM00312H

efficient multifunctional catalyst for urea-water electrolysis. Appl, Cata, B 2024;342:123295.

[81] Bhattacharjee S, Waghmare UV, Lee S-C. An improved d-band model of the catalytic activity of magnetic transition metal surfaces. Scientific Reports 2016;6:35916.

[82] Dickens CF, Montoya JH, Kulkarni AR, Bajdich M, Nørskov JK. An electronic structure descriptor for oxygen reactivity at metal and metal-oxide surfaces. Surf Sci 2019;681:122-9.

[83] Danilovic N, Subbaraman R, Strmcnik D, Chang K-C, Paulikas AP, Stamenkovic VR, et al. Enhancing the Alkaline Hydrogen Evolution Reaction Activity through the Bifunctionality of $Ni(OH)_2$/Metal Catalysts. Angewandte Chemie International Edition 2012;51:12495-8.

[84] Trasatti S. Work function, electronegativity, and electrochemical behaviour of metals: III. Electrolytic hydrogen evolution in acid solutions. Journal of Electroanalytical Chemistry and Interfacial Electrochemistry 1972;39:163-84.

[85] Li N, Zhang L, Wang Y, Zhou S, Zhang Y, Abdukayum A, et al. Effect of in-plane Mott-Schottky on the hydroxyl deprotonation in MoS_2@Co_3S_4/NC heterostructure for efficient overall water splitting. J Colloid Interface Sci 2023;649:125-31.

[86] Zhang K, Guo F, Graham N, Yu W. Engineering Morphology and Electron Redistribution of a Ni/WO3 Mott–Schottky Bifunctional Electrocatalyst for Efficient Alkaline Urea Splitting. ACS Appl Mater Interfaces 2023;15:50116-25.

[87] Li T, Kasian O, Cherevko S, Zhang S, Geiger S, Scheu C, et al. Atomic-scale insights into surface species of electrocatalysts in three dimensions. Nature Catalysis 2018;1:300-5.

[88] Chai G-L, Hou Z, Shu D-J, Ikeda T, Terakura K. Active Sites and Mechanisms for Oxygen Reduction Reaction on Nitrogen-Doped Carbon Alloy Catalysts: Stone–Wales Defect and Curvature Effect. J Am Chem Soc 2014;136:13629-40.

[89] Sun Z, Wang Y, Zhang L, Wu H, Jin Y, Li Y, et al. Simultaneously Realizing Rapid Electron

Transfer and Mass Transport in Jellyfish-Like Mott–Schottky Nanoreactors for Oxygen Reduction Reaction. Adv Funct Mater 2020;30:1910482.

View Article Online
DOI: 10.1039/D4QM00312H

[90] Peng L, Su L, Yu X, Wang R, Cui X, Tian H, et al. Electron redistribution of ruthenium-tungsten oxides Mott-Schottky heterojunction for enhanced hydrogen evolution. Appl, Cata, B 2022;308:121229.

[91] Qiao D, Yun S, Sun M, Dang J, Zhang Y, Yuan S, et al. 1D/3D trepang-like N-modified carbon confined bimetal carbides and metal cobalt: Boosting electron transfer via dual Mott-Schottky heterojunctions triggered built-in electric fields for efficient hydrogen evolution and tri-iodide reduction. Appl, Cata, B 2023;334:122830.

[92] Jiang J, Sun R, Huang X, Xu W, Zhou S, Wei Y, et al. In-situ derived Mo-doped NiCoP and MXene to form Mott-Schottky heterojunction with tunable surface electron density to promote overall water splitting. Composites Part B: Engineering 2023;263:110834.

[93] Li T, Yin J, Sun D, Zhang M, Pang H, Xu L, et al. Manipulation of Mott−Schottky Ni/CeO_2 Heterojunctions into N-Doped Carbon Nanofibers for High-Efficiency Electrochemical Water Splitting. Small 2022;18:2106592.

[94] Esmaili H, Kowsari E, Ramakrishna S. Significance of nanostructure morphologies in photoelectrochemical water splitting cells: A brief review. J Mol Struct 2021;1230:129856.

[95] Xue Z-H, Su H, Yu Q-Y, Zhang B, Wang H-H, Li X-H, et al. Janus Co/CoP Nanoparticles as Efficient Mott–Schottky Electrocatalysts for Overall Water Splitting in Wide pH Range. Adv Energy Mater 2017;7:1602355.

[96] Hou J, Sun Y, Wu Y, Cao S, Sun L. Promoting Active Sites in Core–Shell Nanowire Array as Mott–Schottky Electrocatalysts for Efficient and Stable Overall Water Splitting. Adv Funct Mater 2018;28:1704447.

View Article Online
DOI: 10.1039/D4QM00312H

[97] Nasser R, Zhou H, Elhouichet H, Melhi S, Li Z, Song J-M. $NiFe_2O_4$@$NiCo_2O_4$ hollow algae-like microspheres enabled by Mott-Schottky for electrochemical energy storage. Chem Eng J 2024;489:151554.

[98] Xia S, Zhou Q, Sun R, Chen L, Zhang M, Pang H, et al. In-situ immobilization of CoNi nanoparticles into N-doped carbon nanotubes/nanowire-coupled superstructures as an efficient Mott-Schottky electrocatalyst toward electrocatalytic oxygen reduction. Chinese Journal of Catalysis 2023;54:278-89.

[99] Chen J, Zheng J, He W, Liang H, Li Y, Cui H, et al. Self-standing hollow porous Co/a-WO_x nanowire with maximum Mott-Schottky effect for boosting alkaline hydrogen evolution reaction. Nano Res 2023;16:4603-11.

[100] Zhu Y, Lin Q, Zhong Y, Tahini HA, Shao Z, Wang H. Metal oxide-based materials as an emerging family of hydrogen evolution electrocatalysts. Energy Environ Sci 2020;13:3361-92.

[101] Li Y, Sun Y, Qin Y, Zhang W, Wang L, Luo M, et al. Recent Advances on Water-Splitting Electrocatalysis Mediated by Noble-Metal-Based Nanostructured Materials. Adv Energy Mater 2020;10:1903120.

[102] Sun M, Yun S, Dang J, Zhang Y, Liu Z, Qiao D. 1D/3D rambutan-like Mott–Schottky porous carbon polyhedrons for efficient tri-iodide reduction and hydrogen evolution reaction. Chem Eng J 2023;458:141301.

[103] Chen X, Shi D, Bi M, Song J, Qin Y, Du S, et al. Constructing built-in electric field via ruthenium/cerium dioxide Mott-Schottky heterojunction for highly efficient electrocatalytic hydrogen production. J Colloid Interface Sci 2023;652:653-62.

[104] Wang N, Ning S, Yu X, Chen D, Li Z, Xu J, et al. Graphene composites with Ru-RuO_2 heterostructures: Highly efficient Mott–Schottky-type electrocatalysts for pH-universal water

splitting and flexible zinc–air batteries. Appl, Cata, B 2022;302:120838.

[105] Liu Y, Liu S, Wang Y, Zhang Q, Gu L, Zhao S, et al. Ru Modulation Effects in the Synthesis of Unique Rod-like Ni@Ni_2P–Ru Heterostructures and Their Remarkable Electrocatalytic Hydrogen Evolution Performance. J Am Chem Soc 2018;140:2731-4.

[106] Pu Z, Amiinu IS, Kou Z, Li W, Mu S. RuP_2-Based Catalysts with Platinum-like Activity and Higher Durability for the Hydrogen Evolution Reaction at All pH Values. Angewandte Chemie International Edition 2017;56:11559-64.

[107] Zhou G, Zhang S, Zhu Y, Li J, Sun K, Pang H, et al. Manipulating the Rectifying Contact between Ultrafine Ru Nanoclusters and N-Doped Carbon Nanofibers for High-Efficiency pH-Universal Electrocatalytic Hydrogen Evolution. Small 2023;19:2206781.

[108] Li C, Liu Y, Zhuo Z, Ju H, Li D, Guo Y, et al. Local Charge Distribution Engineered by Schottky Heterojunctions toward Urea Electrolysis. Adv Energy Mater 2018;8:1801775.

[109] Sarkar B, Das D, Nanda KK. pH-dependent hydrogen evolution using spatially confined ruthenium on hollow N-doped carbon nanocages as a Mott–Schottky catalyst. J Mater Chem A 2021;9:13958-66.

[110] Luo Q, Lu C, Liu L, Zhu M. A review on the synthesis of transition metal nitride nanostructures and their energy related applications. Green Energy & Environment 2023;8:406-37.

[111] Wang Z-L, Hao X-F, Jiang Z, Sun X-P, Xu D, Wang J, et al. C and N Hybrid Coordination Derived Co–C–N Complex as a Highly Efficient Electrocatalyst for Hydrogen Evolution Reaction. J Am Chem Soc 2015;137:15070-3.

[112] Xie C, Smaligo AJ, Song X-R, Kwon O. Phosphorus-Based Catalysis. ACS Central Science 2021;7:536-58.

[113] Chen Z, Song Y, Cai J, Zheng X, Han D, Wu Y, et al. Tailoring the d-Band Centers Enables

View Article Online
DOI: 10.1039/D4QM00312H

Co_4N Nanosheets To Be Highly Active for Hydrogen Evolution Catalysis. Angewandte Chemie International Edition 2018;57:5076-80.

[114] Jin H, Liu X, Vasileff A, Jiao Y, Zhao Y, Zheng Y, et al. Single-Crystal Nitrogen-Rich Two-Dimensional Mo_5N_6 Nanosheets for Efficient and Stable Seawater Splitting. ACS Nano 2018;12:12761-9.

[115] Zhou D, Wang S, Jia Y, Xiong X, Yang H, Liu S, et al. NiFe hydroxide lattice tensile strain: enhancement of adsorption of oxygenated intermediates for efficient water oxidation catalysis. Angew Chem Int Ed 2019;58:736-40.

[116] Ye S, Luo F, Xu T, Zhang P, Shi H, Qin S, et al. Boosting the alkaline hydrogen evolution of Ru nanoclusters anchored on B/N–doped graphene by accelerating water dissociation. Nano Energy 2020;68:104301.

[117] Ye S, Luo F, Xu T, Zhang P, Shi H, Qin S, et al. Boosting the alkaline hydrogen evolution of Ru nanoclusters anchored on B/N–doped graphene by accelerating water dissociation. Nano Energy 2020;68:104301.

[118] McCrum IT, Koper M. The role of adsorbed hydroxide in hydrogen evolution reaction kinetics on modified platinum. Nat Energy 2020;5:891-9.

[119] McAllister J, Bandeira NAG, McGlynn JC, Ganin AY, Song Y-F, Bo C, et al. Tuning and mechanistic insights of metal chalcogenide molecular catalysts for the hydrogen-evolution reaction. Nat Commun 2019;10:370.

[120] Chen B, Hu P, Yang F, Hua X, Yang FF, Zhu F, et al. In Situ Porousized MoS_2 Nano Islands Enhance HER/OER Bifunctional Electrocatalysis. Small 2023;19:2207177.

[121] Jin Q, Liu N, Dai C, Xu R, Wu B, Yu G, et al. H_2-Directing Strategy on In Situ Synthesis of Co-MoS_2 with Highly Expanded Interlayer for Elegant HER Activity and its Mechanism. Adv Energy

Mater 2020;10:2000291.

View Article Online
DOI: 10.1039/D4QM00312H

[122] Pi C, Li X, Zhang X, Song H, Zheng Y, Gao B, et al. In-Plane Mott–Schottky Effects Enabling Efficient Hydrogen Evolution from Mo_5N_6-MoS_2 Heterojunction Nanosheets in Universal-pH Electrolytes. Small 2022;18:2201137.

[123] Ye G, Gong Y, Lin J, Li B, He Y, Pantelides ST, et al. Defects Engineered Monolayer MoS_2 for Improved Hydrogen Evolution Reaction. Nano Lett 2016;16:1097-103.

[124] Zhang J, Wang T, Pohl D, Rellinghaus B, Dong R, Liu S, et al. Interface Engineering of MoS_2/Ni_3S_2 Heterostructures for Highly Enhanced Electrochemical Overall-Water-Splitting Activity. Angewandte Chemie International Edition 2016;55:6702-7.

[125] Wu J, Chen T, Zhu C, Du J, Huang L, Yan J, et al. Rational Construction of a WS_2/CoS_2 Heterostructure Electrocatalyst for Efficient Hydrogen Evolution at All pH Values. ACS Sustainable Chem Eng 2020;8:4474-80.

[126] Li S, Zang W, Liu X, Pennycook SJ, Kou Z, Yang C, et al. Heterojunction engineering of $MoSe_2$/MoS_2 with electronic modulation towards synergetic hydrogen evolution reaction and supercapacitance performance. Chem Eng J 2019;359:1419-26.

[127] Rout CS, Joshi PD, Kashid RV, Joag DS, More MA, Simbeck AJ, et al. Superior Field Emission Properties of Layered WS_2-RGO Nanocomposites. Scientific Reports 2013;3:3282.

[128] Chen C-J, Chen P-T, Basu M, Yang K-C, Lu Y-R, Dong C-L, et al. An integrated cobalt disulfide (CoS_2) co-catalyst passivation layer on silicon microwires for photoelectrochemical hydrogen evolution. J Mater Chem A 2015;3:23466-76.

[129] Sun Z, Lin L, Yuan M, Yao H, Deng Y, Huang B, et al. Mott–Schottky heterostructure induce the interfacial electron redistribution of MoS_2 for boosting pH-universal hydrogen evolution with Pt-like activity. Nano Energy 2022;101:107563.

[130] Yu Z, Li Y, Martin-Diaconescu V, Simonelli L, Ruiz Esquius J, Amorim I, et al. Highly Efficient and Stable Saline Water Electrolysis Enabled by Self-Supported Nickel-Iron Phosphosulfide Nanotubes With Heterointerfaces and Under-Coordinated Metal Active Sites. Adv Funct Mater 2022;32:2206138.

[131] Jia H, Wang H, Yan F, Zhang H, Li Z, Wang J. Unravelling electrocatalytic concerted diatomic-ensembles over superior hydrogen-evolution array structured by NiMo/Mo_2N heteronanojunctions. Appl, Cata, B 2024;343:123362.

[132] Begildayeva T, Theerthagiri J, Lee SJ, Yu Y, Choi MY. Unraveling the Synergy of Anion Modulation on Co Electrocatalysts by Pulsed Laser for Water Splitting: Intermediate Capturing by In Situ/Operando Raman Studies. Small 2022;18:2204309.

[133] Shen S, Hong Y, Zhu F, Cao Z, Li Y, Ke F, et al. Tuning Electrochemical Properties of Li-Rich Layered Oxide Cathodes by Adjusting Co/Ni Ratios and Mechanism Investigation Using in situ X-ray Diffraction and Online Continuous Flow Differential Electrochemical Mass Spectrometry. ACS Appl Mater Interfaces 2018;10:12666-77.

[134] Han MH, Ko Y-J, Lee SY, Lim C, Lee WH, Pin MW, et al. Thermo-selenized stainless steel as an efficient oxygen evolution electrode for water splitting and CO2 electrolysis in real water matrices. J Power Sources 2022;521:230953.

[135] Jang D, Kim J, Kim D, Han W-B, Kang S. Techno-economic analysis and Monte Carlo simulation of green hydrogen production technology through various water electrolysis technologies. Energy Convers Manage 2022;258:115499.

[136] Umer M, Umer S, Zafari M, Ha M, Anand R, Hajibabaei A, et al. Machine learning assisted high-throughput screening of transition metal single atom based superb hydrogen evolution electrocatalysts. J Mater Chem A 2022;10:6679-89.

View Article Online
DOI: 10.1039/D4QM00312H

View Article Online
DOI: 10.1039/D4QM00312H

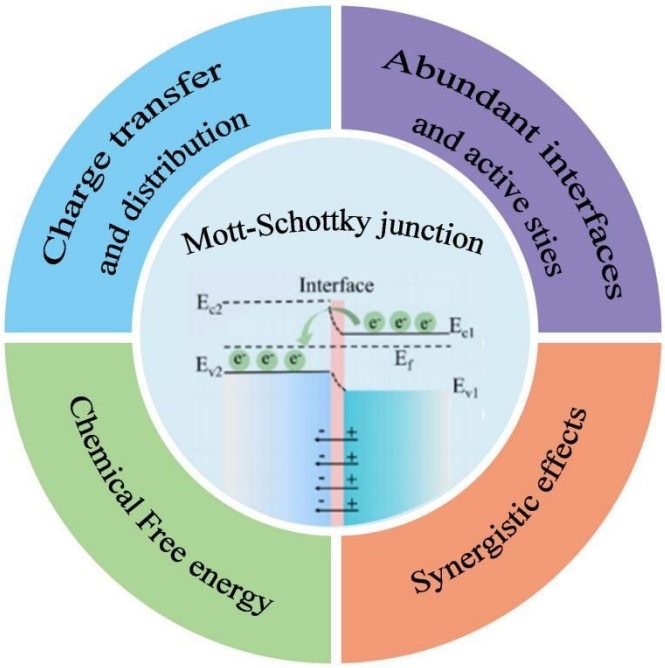

Scheme 1 Schematic illustration of the Mott-Schottky junction in electrocatalysts.

View Article Online
DOI: 10.1039/D4QM00312H

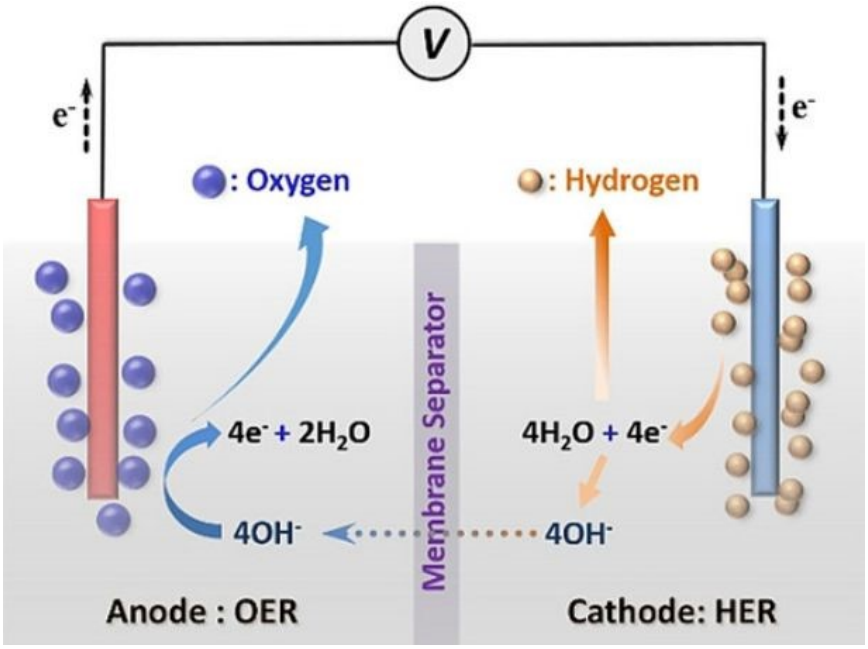

Figure 1 A typical water electrolysis cell under alkaline conditions.

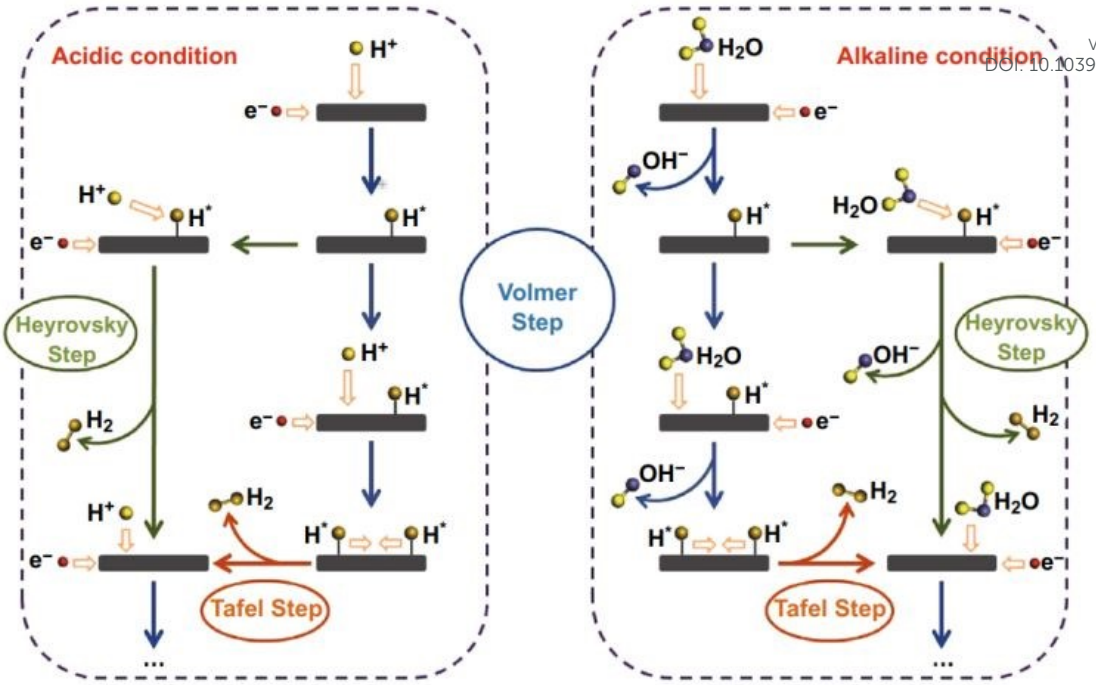

Figure 2 Pathways for hydrogen evolution reaction under acidic and alkaline (or neutral) conditions. Reproduced with permission from Ref. [40]. Copyright 2018, Springer Nature.

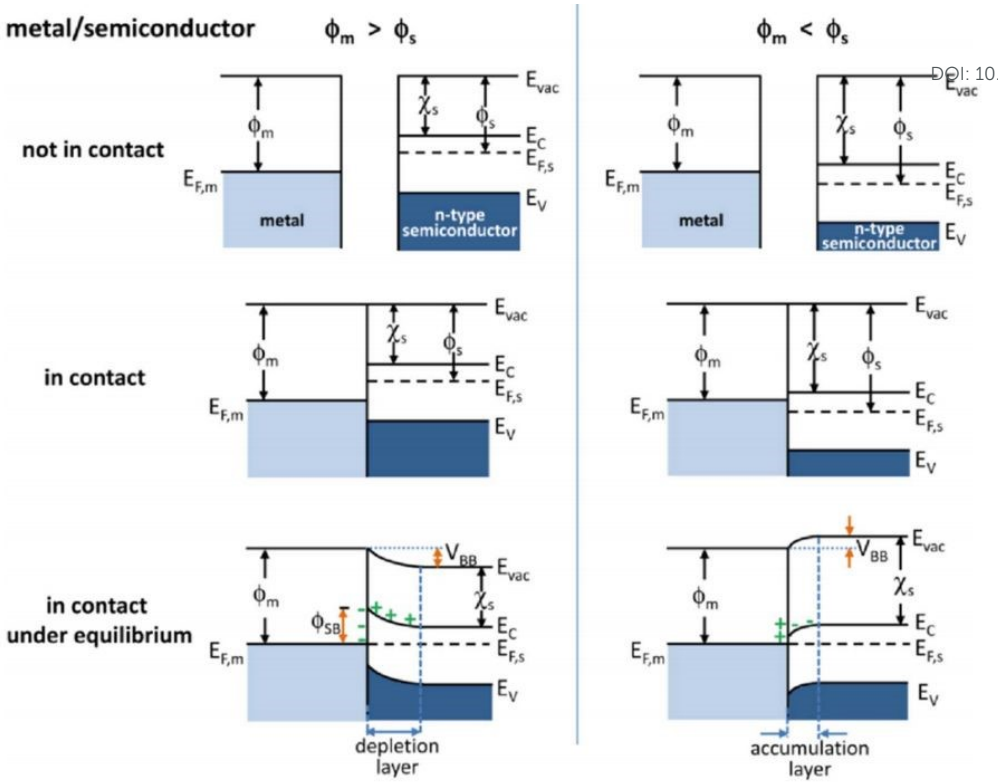

Figure 3 Energy band diagrams of metal and n-type semiconductor contacts. E_{vac}, vacuum energy; E_c, energy of conduction band minimum; E_v, energy of valence band maximum; $E_{F,\,s}$, Fermi level; ϕ_m, metal work function; ϕ_s, semiconductor work function; χ_s, electron affinity of the semiconductor. Reproduced with permission.[57] Copyright 2012, American Chemical Society.

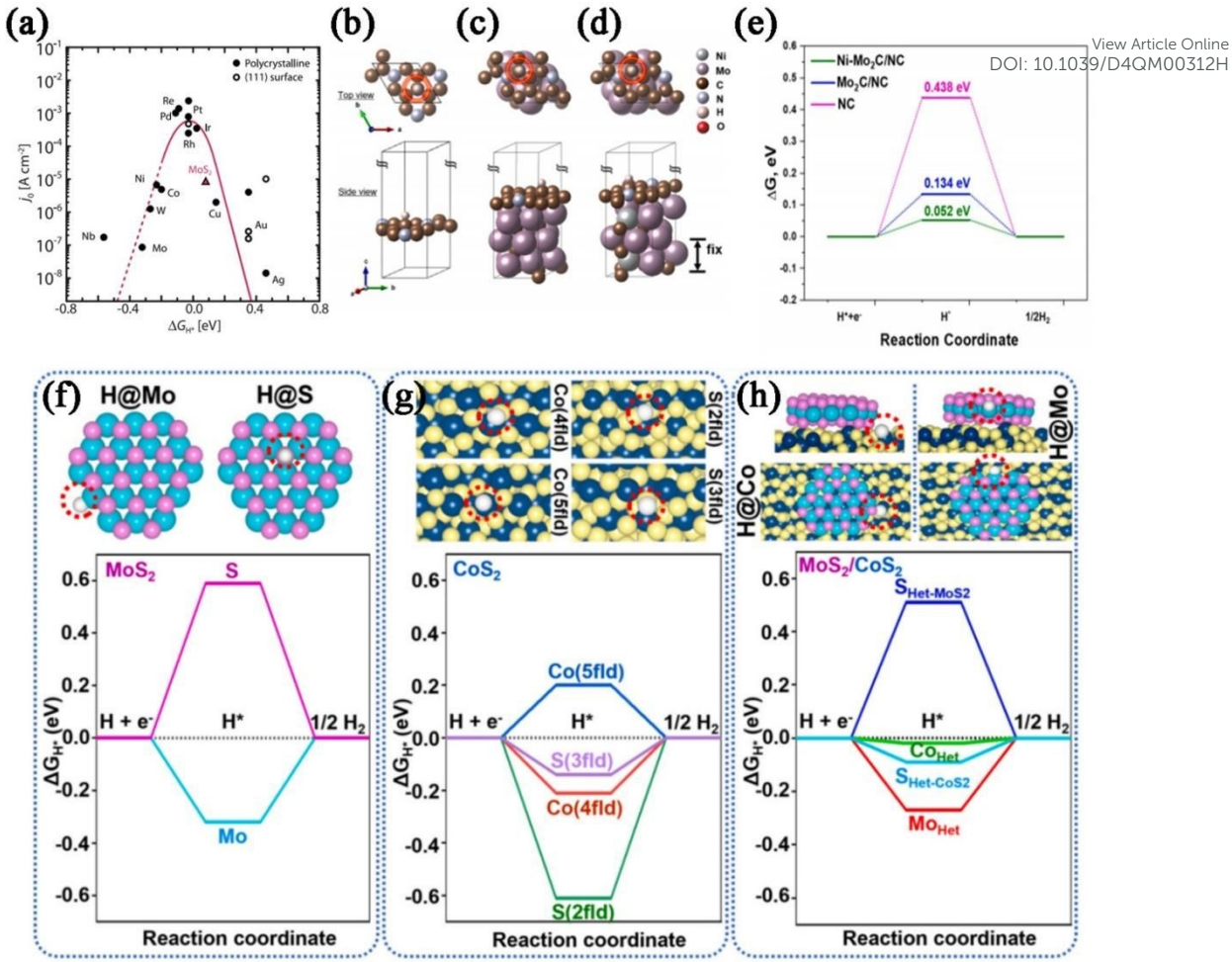

Figure 4 (a) Hydrogen free binding energy versus activity. Circles represent experimental data, and the curve is from microkinetic theory. Reproduced with permission.[68] Copyright 2010, American Association for the Advancement of Science. The most stable adsorption site of H* on (b) NC, (c) Mo_2C/NC, and (d) Ni-Mo_2C/NC. (e) The HER free energy diagram for NC, Mo_2C/NC and Ni-Mo_2C/NC. Reproduced with permission.[67] Copyright 2021, Elsevier.(f)-(h) The Gibbs free energy diagram of HER at different H adsorption sites on the surface of MoS_2, CoS_2, and MoS_2/CoS_2, respectively. Reproduced with permission.[71] Copyright 2024, Elsevier.

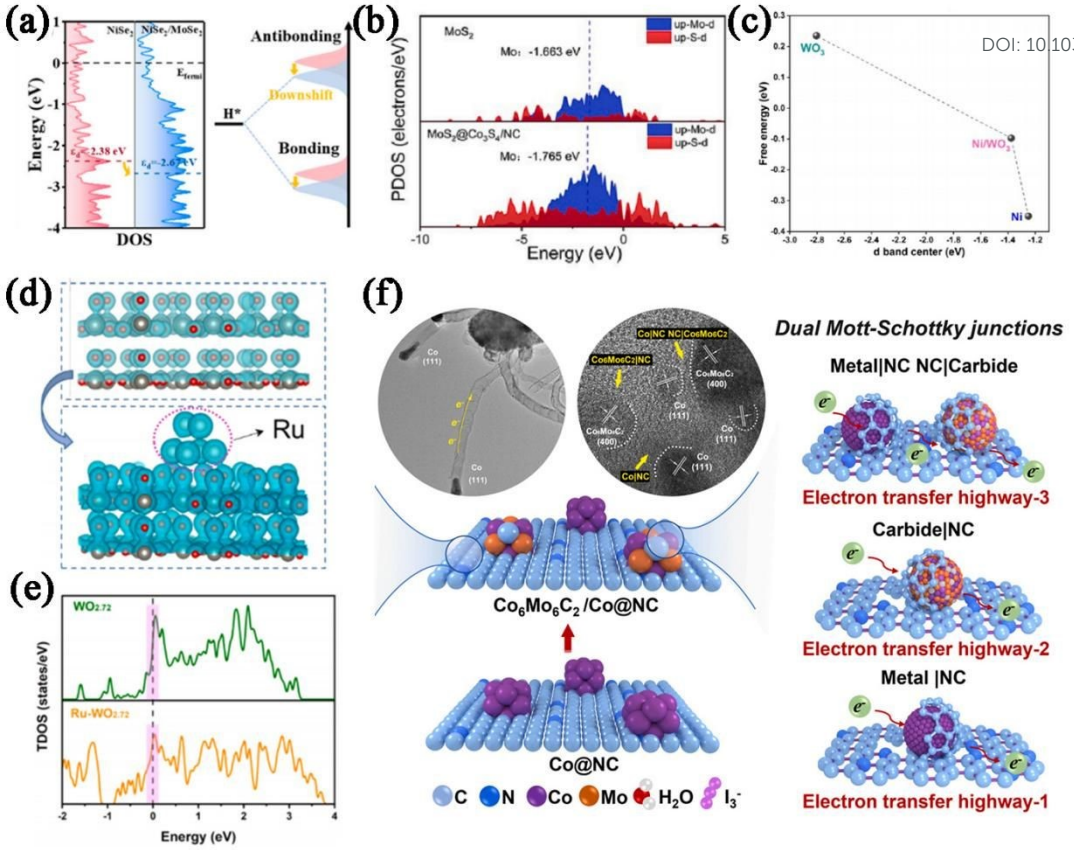

Figure 5 (a) The density of states of $NiSe_2$ and $NiSe_2/MoSe_2$, and the schematic illustration of the bond formation between the catalyst surface and H*. The d-band centers are also shown.Reproduced with permission.[31] Copyright 2024, Elsevier. (b)PDOS plots of the Mo site of MoS_2 and $MoS_2@Co_3S_4/NC$ heterointerfaces. Reproduced with permission.[76] Copyright 2023, Elsevier. (c)Dependence of free energies of hydrogen adsorption on the d-band centers (ε_d) of WO_3, Ni, and Ni/WO_3.Reproduced with permission.[77] Copyright 2023, American Chemical Society. (d) Calculated charge density difference of $WO_{2.72}$ (up) and WR (down). (e) Calculated DOS of $WO_{2.72}$ and WR. Reproduced with permission.[81] Copyright 2022, Elsevier. (f) The schematic illustration of 1D/3D-structured dual Mott-Schottky heterojunctions (Co|NC and $Co_6Mo_6C_2|NC$) in $Co_6Mo_6C_2/Co@NC$ (electron transfer highway-1: Co→NC; highway-2: NC→$Co_6Mo_6C_2$; highway-3: Co→NC→$Co_6Mo_6C_2$). Reproduced with permission.[82] Copyright 2023, Elsevier.

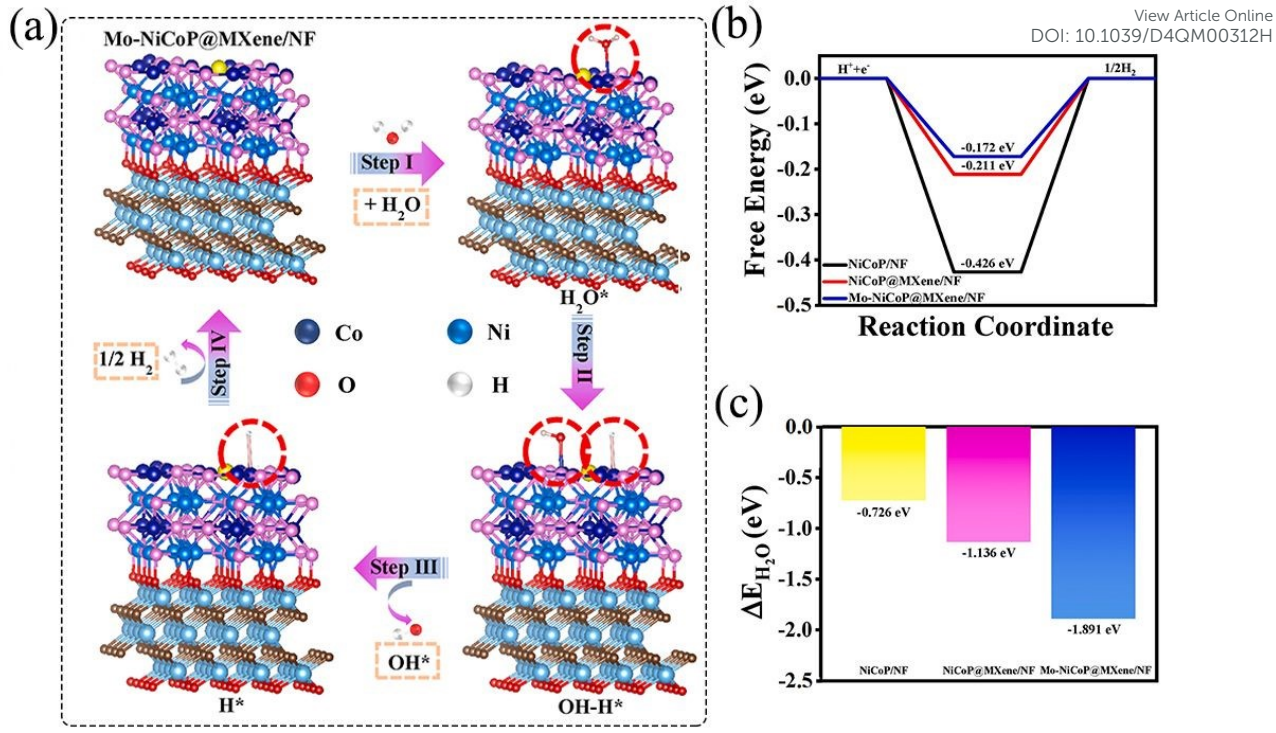

Figure 6 (a) The HER process and optimization model for adsorbed intermediates of Mo-NiCoP@MXene/NF. (b) Calculated ΔG_{H^*} of Mo-NiCoP@MXene/NF and comparative samples; (c) Adsorption energy of H_2O on the NiCoP/NF, NiCoP@MXene/NF, and Mo-NiCoP@MXene/NF samples. Reproduced with permission.[92] Copyright 2023, Elsevier.

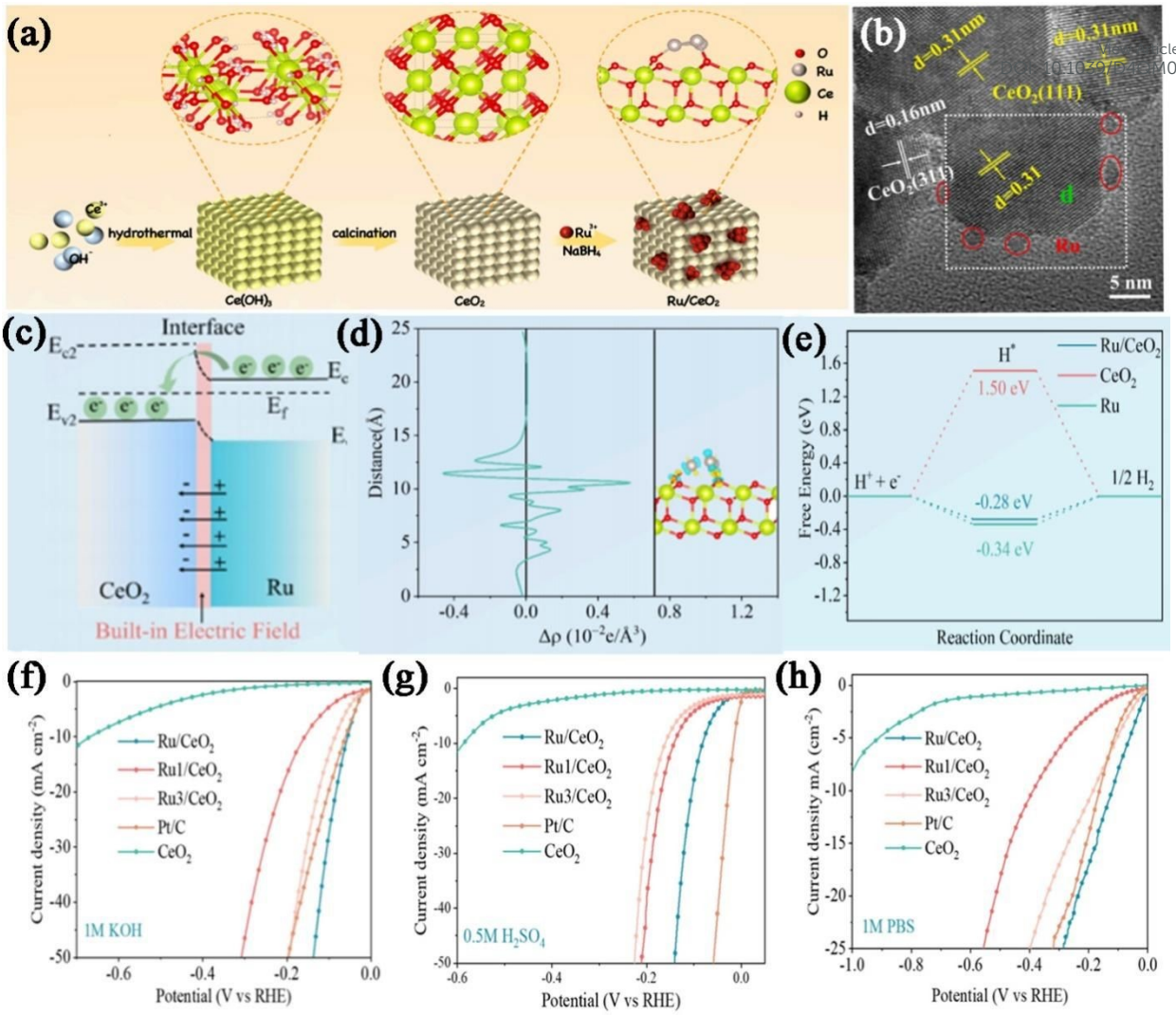

Figure 7 (a) Schematic diagram of the synthesis process of Ru/CeO_2. (b) HRTEM images of Ru/CeO_2. (c) Schematic diagram of the Mott-Schottky heterojunction. (d) The planar-averaged electron density difference (Δρ) and corresponding side view of the electron density difference over Ru/CeO_2. (e) Gibbs free energy diagram of the CeO_2 (111) plane, Ru (101) plane, and Ru/CeO_2. (f-h) LSV curves of different catalysts in (f) 1M KOH (g) 0.5 M H_2SO_4 and (h) 1 M PBS. Reproduced with permission.[86] Copyright 2023, Elsevier.

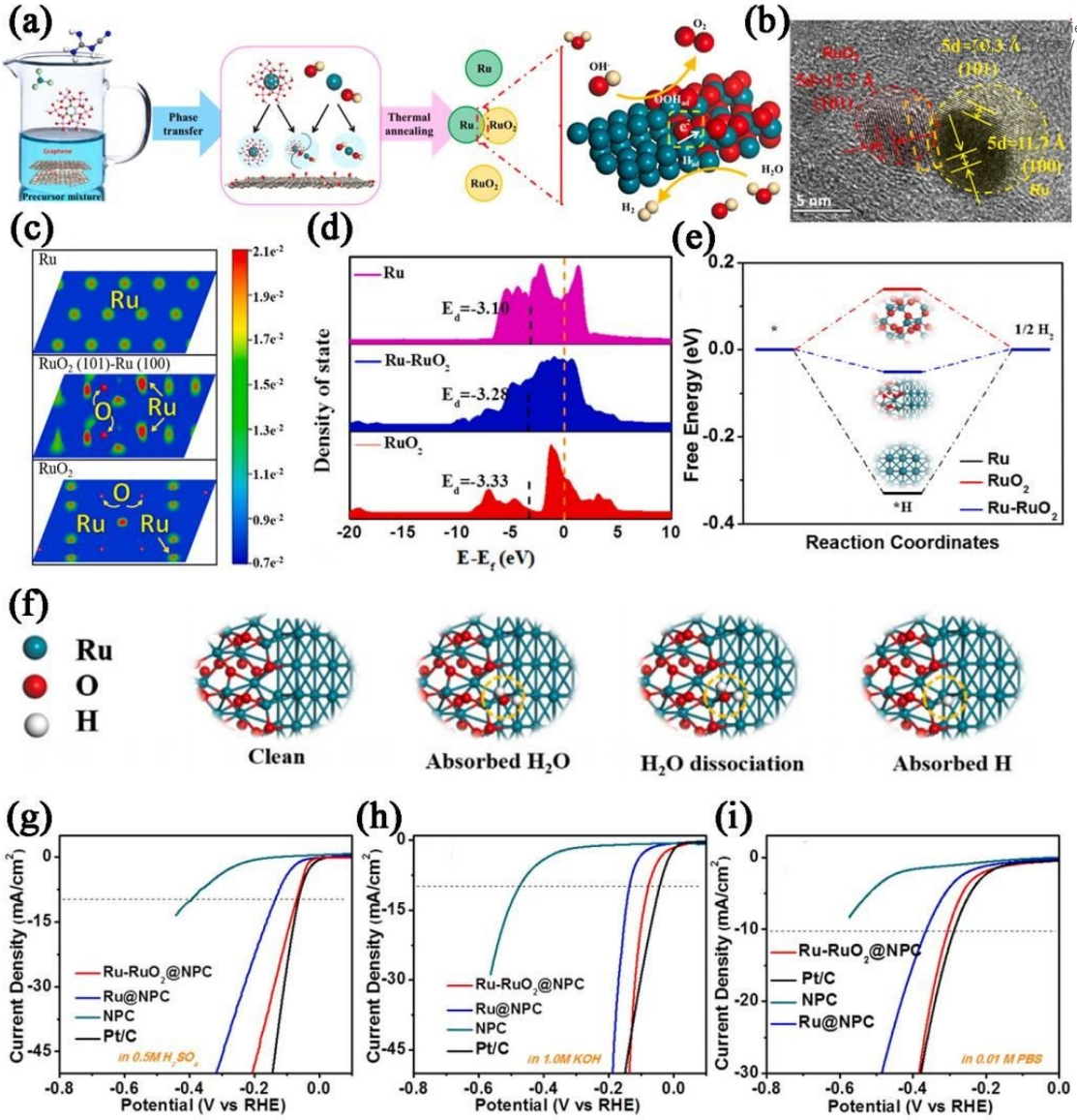

Figure 8 (a) Schematic depiction of the synthesis of Ru-RuO_2@NPC nanocomposites. (b) High-resolution TEM image of the selected area in panel. (c) Projected DOS and d band of RuO_2 and Ru-RuO_2. (d) energetic pathway of HER. (b) Atomic configurations of the water dissociation step on the surface of the Ru-RuO_2 Mott–Schottky-Type heterostructure, including H_2O adsorption, activated H_2O adsorption, OH adsorption and H adsorption. (e-g) HER in (g) 0.5 M H_2SO_4 solution, (h) 1.0 M KOH solution and (i) 0.01 M PBS solution, respectively. Reproduced with permission.[88] Copyright 2022, Elsevier.

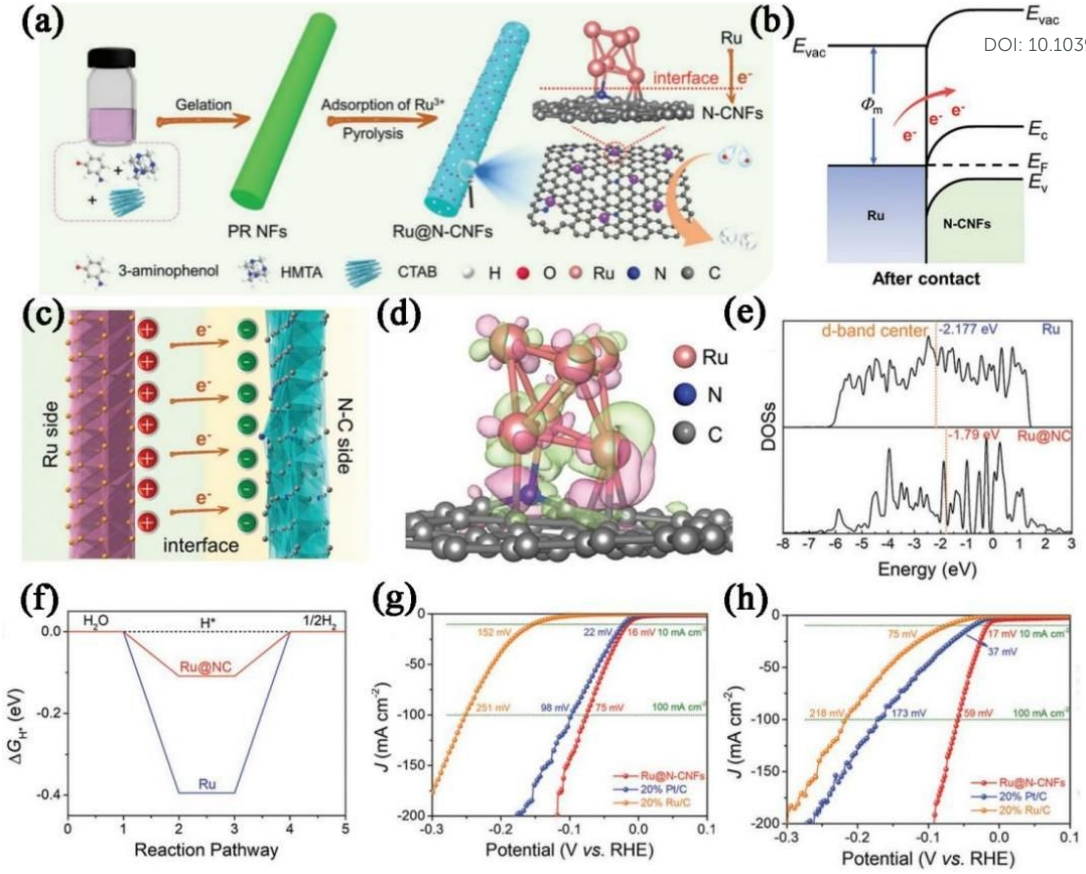

Figure 9 (a) Schematic illustration for the preparation of Ru@N-CNFs. (b) energy band diagrams of Ru and N-CNFs after rectifying contact. c) the schematic diagram for the charge transfer between Ru and N-CNFs. d) Charge density difference at the heterointerface between Ru and NC. d) DOSs distributions, e) ΔG_{H^*} iagrams of Ru and Ru@NC. (g-h)Comparison of HER performances of different catalysts in g) acidic and h) alkaline electrolytes. Reproduced with permission.[91] Copyright 2023, Wiley.

.

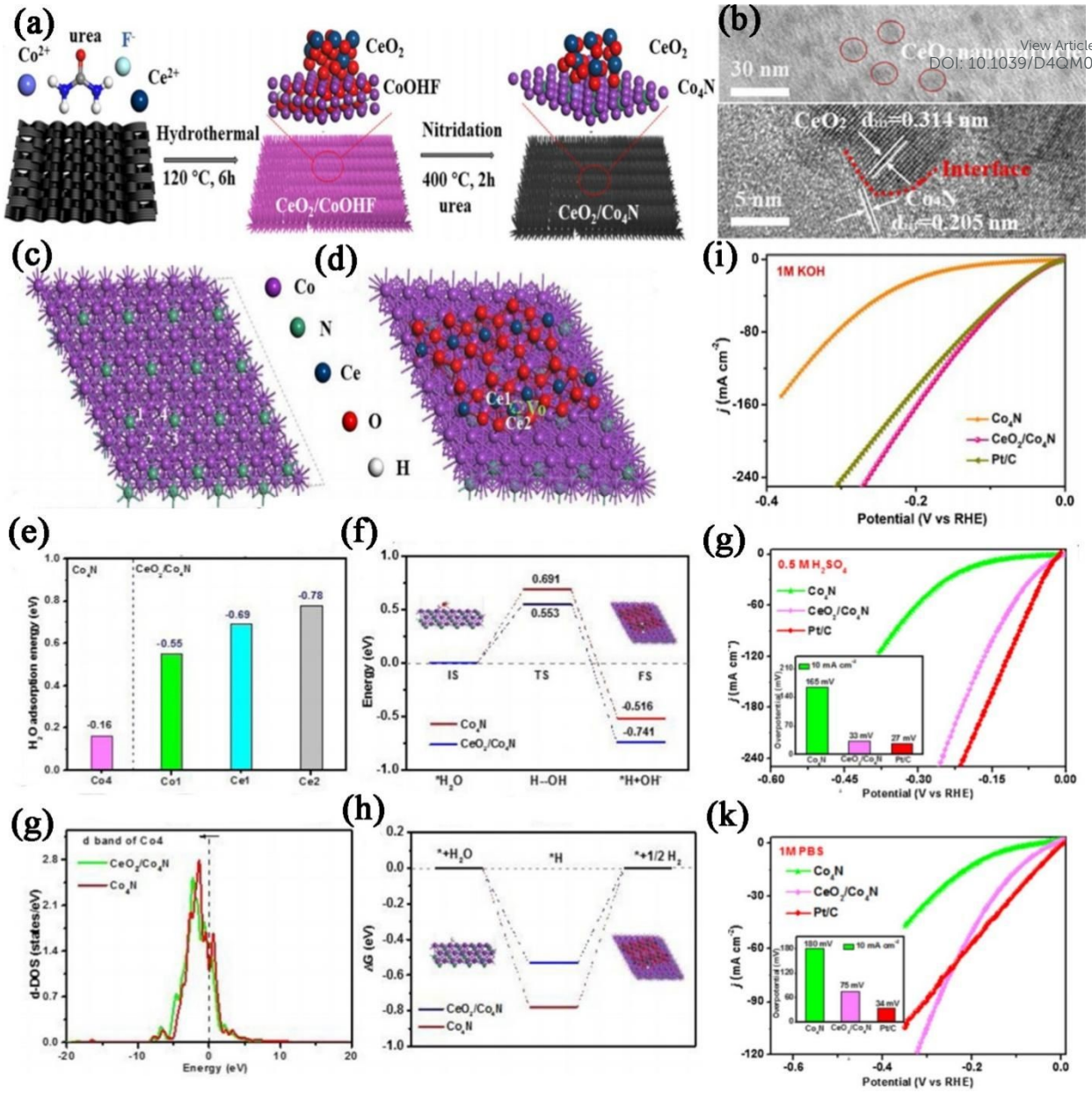

Figure 10 (a) The synthetic methods of CeO_2/Co_4N; (b) TEM images (up) and HRTEM image (down) of CeO_2/Co_4N; (c) The geometric configuration of Co_4N (111) surface and (d) Vo-CeO_2 (111)/Co_4N (111) heterogeneous structure surface; (e) The Gibbs adsorption free energies of water on Co_4N and CeO_2/Co_4N (111) surface; (f) The calculated water dissociation barriers on CeO_2/Co_4N and Co_4N, respectively; (g) The calculated density of states (DOS) of Co_4N and CeO_2/Co_4N; (h) Free energy diagram of HER on Co_4N and Vo-CeO_2/Co_4N; (i-k) HER in (i) 1 M KOH solution,(j) 0.5 M H_2SO_4 solution and (k) 1 M PBS solution (Inset: Histogram of corresponding LSV curve at current density of 10 mA cm^{-2}).

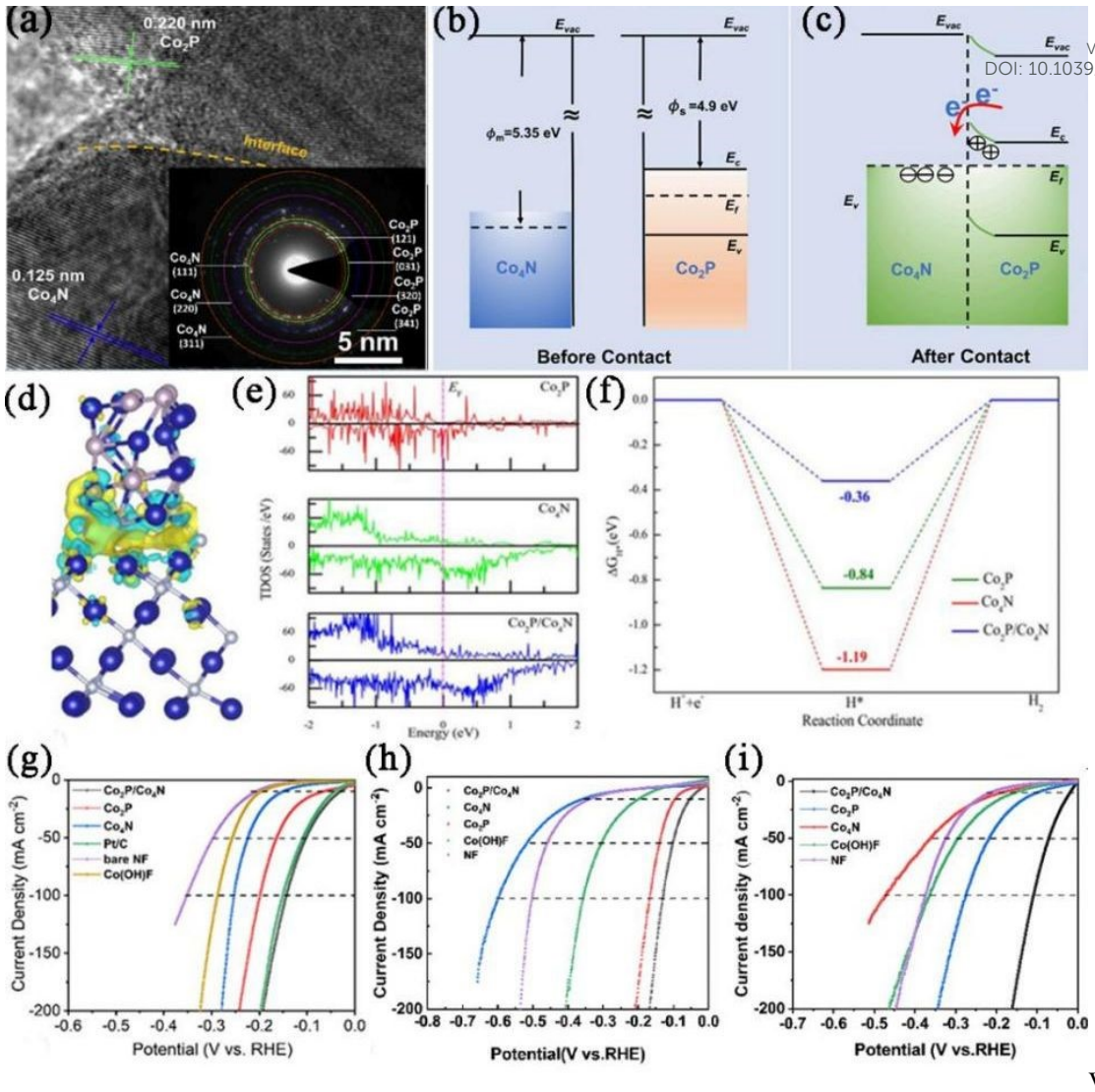

Figure 11 (a) HR-TEM image of Co_2P/Co_4N, (b and c) The proposed energy band diagrams of the metallic Co_4N and Co_2P before contact and after contact (Mott-Schottky heterojunction), where E_F, E_{vac}, E_v and E_c represents the Fermi energy, vacuum energy, valence band and conduction band potentials, respectively. (d) The charge density distribution of Co_2P/Co_4N, (e) the DOSs of Co_2P, Co_4N and Co_2P/Co_4N, (f) The calculated ΔG_{H^*} at the relative stable sites on Co_2P, Co_4N and Co_2P/Co_4N, (g) (h) and (i) are the Polarization curves of different catalysts in 1 M KOH, 0.5 M H_2SO_4 and 1 M PBS, respectively. Reproduced with permission.[22] Copyright 2023, Elsevier.

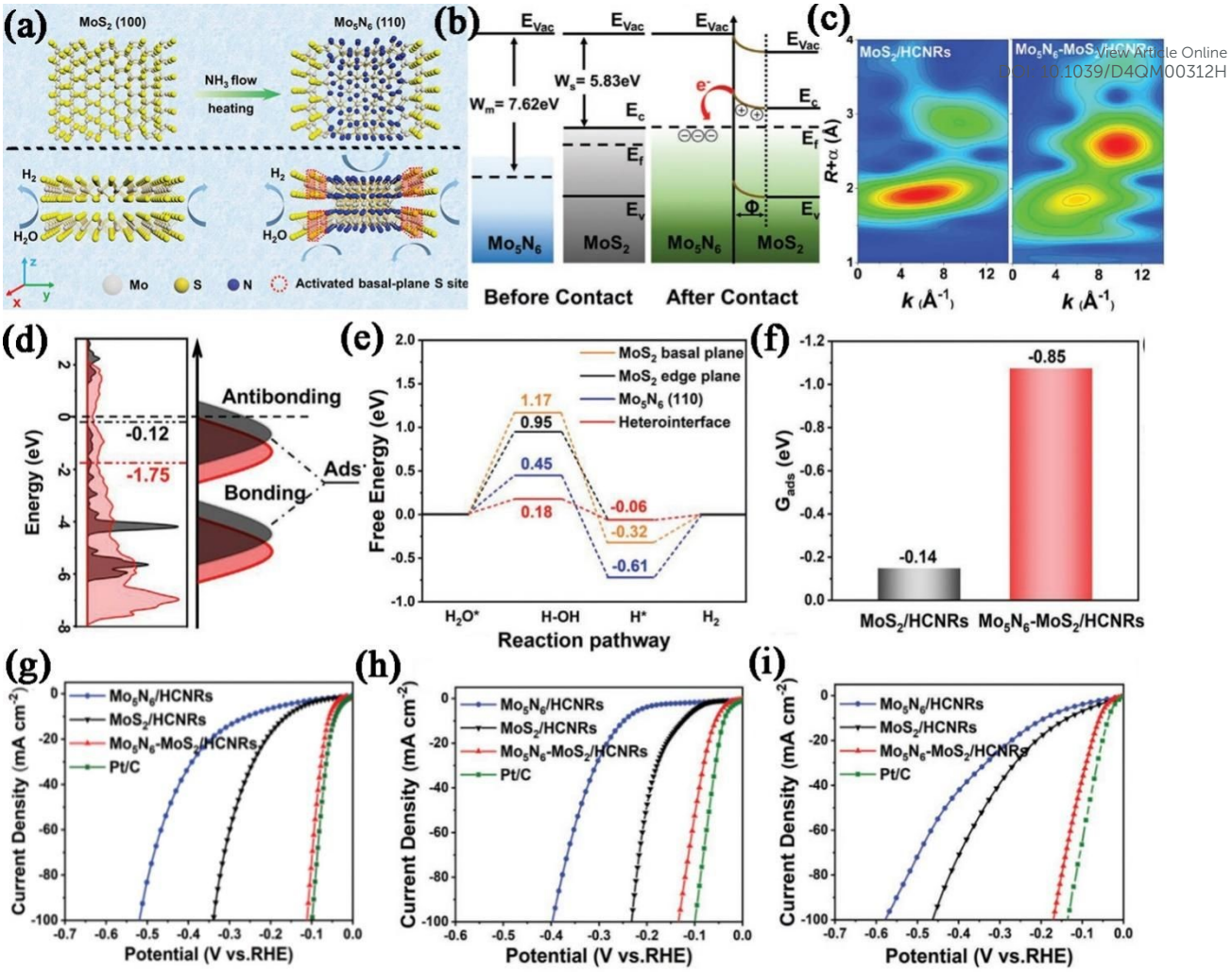

Figure 12 (a) Schematic diagram of the transformation from 2D MoS_2 to in-plane Mo_5N_6-MoS_2 heterojunction (up) and the comparison of active sites to boost HER of 2D MoS_2 and Mo_5N_6-MoS_2 heterojunction (down). (b) Schematic diagrams of energy band of Schottky-type Mo_5N_6-MoS_2 heterojunction. (c) WT-EXAFS of 2H-MoS_2/HCNRs and Mo_5N_6-MoS_2/HCNRs. (d) DOS plots of the Mo site of 2H-MoS_2 and Mo_5N_6-MoS_2 heterointerface, and schematic illustration of bond formation between the surface and adsorbate H*. (e) Energy profiles for water dissociation and free energy diagrams for HER on 2H-MoS_2 basal plane, 2H-MoS_2 edge plane, Mo_5N_6 (110), and Mo_5N_6-MoS_2 heterointerface. (f) H_2O adsorption energy on Mo_5N_6-MoS_2/HCNRs and 2H-MoS_2/HCNRs. (g) (h) and (i) shown the electrocatalytic HER performances of different catalysts in 1 M KOH, 0.5 M H_2SO_4 and 1 M PBS, respectively. Reproduced with permission.[106] Copyright 2022, Wiley.

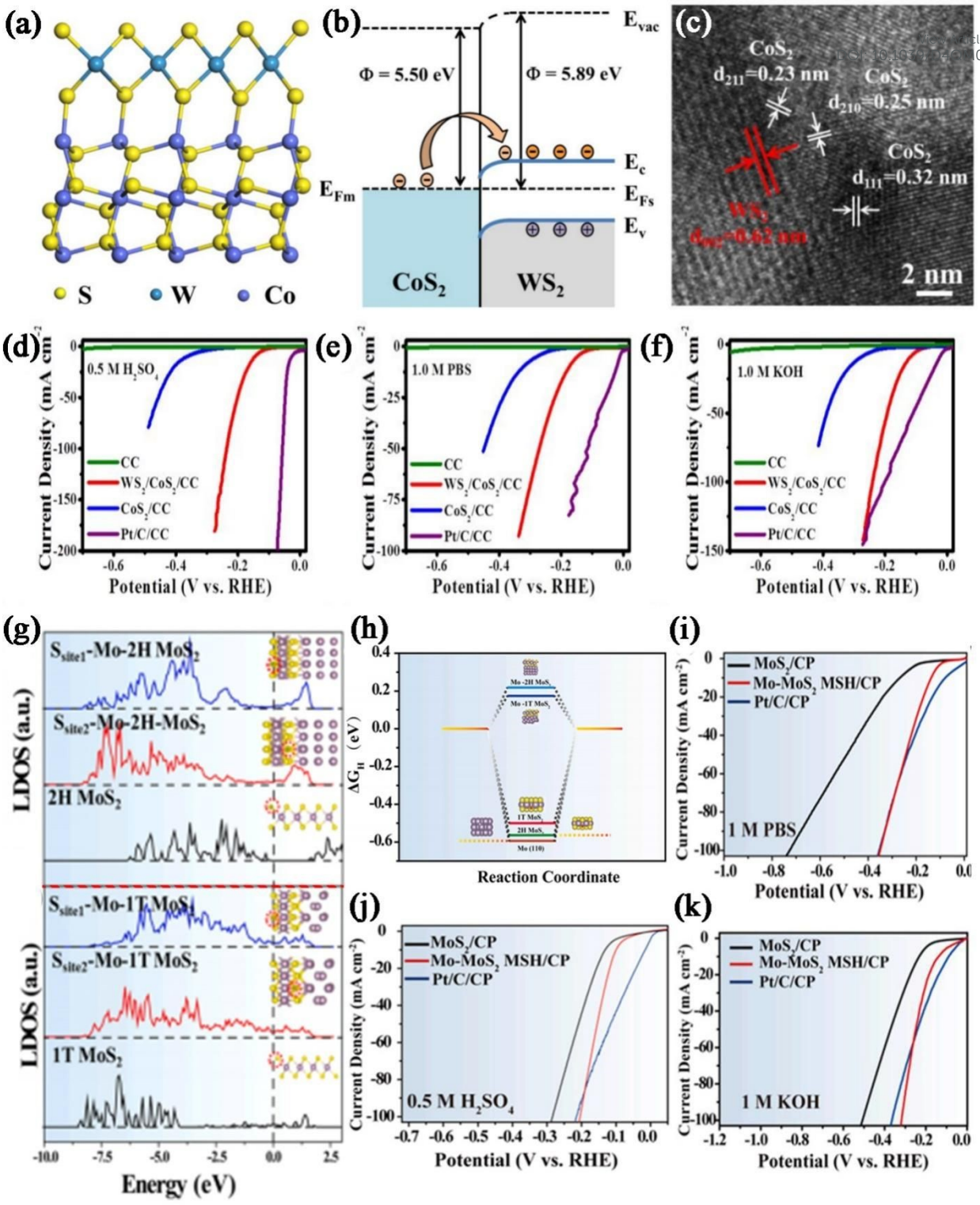

Figure 13 (a) Schematic illustration of WS_2/CoS_2 heterostructure. (b) Schematic energy band diagrams of WS_2/CoS_2 heterostructure in equilibrium. (c) High resolution TEM images of WS_2/CoS_2 heterostructure. (d-f) IR-compensated LSV curves different catalysts after normalizing the currents to the geometric area in different electrolyte. Reproduced with permission.[109] Copyright 2020, American Chemical Society. (g) The LDOS for different S sites of 2H MoS_2 and Mo-2H MoS_2 MSH (up) and the LDOS for different S sites of 1T MoS_2 and Mo-1T MoS_2 MSH (down). (h) corresponding optimal ΔG_{H^*} for HER. (i-k)Linear sweep voltammetry curves of MoS_2/CP, Mo-MoS_2 MSH/CP and Pt/C/CP in (i) 1.0 M PBS, (j) 0.5 M H_2SO_4 and (k) 1.0 M KOH. Reproduced with permission.[113] Copyright 2020, Elsevier.